

EUROPEAN SCHOOL OF MOLECULAR MEDICINE

PhD in Molecular Medicine (Human Genetics)

XXV Cycle

Telethon Institute of Genetics and Medicine (TIGEM)

Therapeutic approaches to Lysosomal Storage Disorders: the example of Pompe Disease

Supervisor
Prof. Andrea Ballabio

Internal co-supervisor
Prof. Brunella Franco

External co-supervisor
Dr. Maria Pia Cosma

CANDIDATE
Dr. Fabio Annunziata

January 2014

Yesterday is but today`s memory, tomorrow is today`s dream.

Khalil Gibran

*Being with you and not being with you is the only way I have to
measure time*

Jorge Luis Borges

TABLE OF CONTENT

ABSTRACT	1
INTRODUCTION	2
1. Lysosome	2
1.1 General characteristics	2
1.2 Lysosomal membrane structure	3
1.3 Lysosomal content	5
1.4 Transport systems	6
1.5 Lysosomal biogenesis	7
2. Lysosomal Storage Disorders	9
2.1 Multiple Sulfatases Deficiency (MSD)	10
2.2 Mucopolysaccharidosis type IIIA (MPS-III A)	12
2.3 Pompe Disease (PD)	14
3. Therapies for LSDs	15
3.1 Enzyme Replacement Therapy (ERT)	15
3.2 Bone Marrow Transplantation (BMT)	17
3.3 Ex-vivo Gene Therapy	19
3.4 In-vivo Gene Therapy	21
3.5 Enzyme Enhancement Therapy	22
3.6 Substrate Reduction Therapy	23
4. Pathogenesis in LSDs	23
AIM OF THE THESIS	26
RESULTS	28

1. Identification of the molecular pathogenic mechanism in LSDs	28
1.1 Lysosomal fusion is impaired in LSDs	28
1.2 Cholesterol accumulates in the endolysosomal membranes of LSDs reducing the efficiency of lysosomal fusion	30
1.3 The organization of the endolysosomal membranes is altered in LSDs cells	34
1.4 Endolysosomal SNARE membrane compartmentalization is highly dependent on cholesterol and is altered in LSDs cells	38
1.5 Endolysosomal SNAREs are locked in assembled complexes in LSD cells	42
1.6 The traffic and recycling of Post-Golgi endolysosomal SNAREs is inhibited in LSD cells	46
2. Linking the molecular phenotype to the treatment for LSDs	49
2.1 TFEB overexpression reduces lysosomal size and glycogen burden in PD myotubes	50
2.2 TFEB overexpression in PD muscle induces cellular clearance by promoting lysosomal/autophagosomal exocytosis	54
2.3 Suppression of autophagy attenuates TFEB-mediated cellular clearance in PD muscle	59
2.4 Intramuscular injection of AAV2.1-TFEB results in clearance of glycogen stores and amelioration of muscle pathology	62
DISCUSSION	67
MATERIAL AND METHODS	73
BIBLIOGRAPHY	88

FIGURE INDEX

Fig.1 EGFR degradation is impaired in LSD cells	28
Fig.2 Dextran uptake is impaired in LSD cells	29
Fig.3 Lysosomal fusion is impaired in LSD cells	30
Fig.4 Cholesterol accumulation in endolysosomal membrane from LSD cells	31
Fig.5 Alteration of lipid composition of endolysosomal membranes from LSD cells	32
Fig.6 Cholesterol modulation in LSD and WT cells	33
Fig.7 Cholesterol accumulation inhibits lysosomal/autophagosomal fusion	34
Fig.8 Cholesterol accumulation inhibits lysosomal/endosomal fusion	34
Fig.9 LSD endolysosomal membrane contains increased amount of detergent resistant Domains (DRMs)	35
Fig.10 The LSD endolysosomal membrane contains increased amount of cholesterol enriched regions	36
Fig.11 The LSD endolysosomal membrane maintains a membrane order similar to WT endolysosomal membranes	36
Fig.12 LSD endolysosomal membranes show an abnormal protein content in LSD cells	37
Fig.13 Protein distribution on endolysosomal membranes is altered in LSD cells	38
Fig.14 SNAREs are sequestered by cholesterol within endolysosomal membranes	39

Fig.15 SNARE proteins are overexpressed on endolysosomal membranes of cholesterol-loaded cells	40
Fig.16 VAMP7 distribution is affected in LSD cells	40
Fig.17 SNARE proteins are overexpressed in cholesterol loaded cells	41
Fig.18 Association with DRM is specific for SNARE proteins in LSD cells	42
Fig.19 SNAREs are locked in high molecular weight complexes in LSD endolysosomal membranes	43
Fig.20 SNARE proteins are locked in assembled form in LSD endolysosomal membranes	44
Fig.21 SNARE complexes in LSD cells are associated to DRMs	45
Fig.22 α -SNAP is more associated with endolysosomal membranes in LSD cells	46
Fig.23 Increased co-localization of SNARE proteins in LSD cells	47
Fig.24 Cholesterol levels affect SNARE localization	48
Fig.25 Cholesterol levels affect SNARE trafficking	49
Fig.26 TFEB stimulates clearance of enlarged lysosomes in PD myotubes	51
Fig.27 TFEB induces relocation of Lysosomes to the plasma membrane in PD myotubes	52
Fig.28 TFEB reduces glycogen burden in PD myotubes	53
Fig.29 TFEBmt reduces lysosomal size in PD myotubes	54
Fig.30 TFEBmt induces apoptosis in a subset of PD myotubes	54

Fig.31 TFEB promotes clearance of enlarged lysosomes in PD fibres	56
Fig.32 TFEB induces lysosomal localization to plasma membrane in PD fibres	56
Fig.33 TFEB increases lysosomal motility in PD fibres	57
Fig.34 TFEB stimulates lysosomal/autophagosomal fusion and clearance	59
Fig.35 TFEB promotes redistribution and docking of lysosomes to the plasma membrane in autophagy-deficient PD fibres	61
Fig.36 TFEB increases lysosomal velocity in autophagy-deficient PD fibres	62
Fig.37 Intramuscular injection of AAV2.1-TFEB in GAA ^{-/-} mice promotes glycogen clearance	63
Fig.38 Intramuscular injection of AAV2.1-TFEB in GAA ^{-/-} mice attenuates PD pathology	63
Fig.39 Intramuscular injection of AAV2.1-TFEB in GAA ^{-/-} mice promotes clearance of enlarged lysosomes	64
Fig.40 Impact of TFEB on muscle fibre ultrastructure in GAA ^{-/-} mice	66

ABSTRACT

Lysosomal Storage Disorders (LSDs) are different inherited diseases caused by the deficit of lysosomal or non-lysosomal proteins, resulting in the accumulation of undegraded substrates in lysosomes. Recent studies support the idea that LSDs are associated with a global impairment of the entire endo-lysosomal compartment, specifically of autophagy involved in the principal lysosome-related degradative pathway. However little is known about the mechanisms underlying such dysfunction. Identification of these mechanisms is crucial for the development of precisely targeted therapies for LSDs.

In this work I demonstrate that secondary accumulation of cholesterol on lysosomal membranes is the principal molecular mechanism at the basis of lysosomal and autophagosomal dysfunction, as it affects the fusogenic ability of lysosomal membranes. Specifically cholesterol overload affects the distribution and function of SNARE proteins, a protein superfamily involved in fusing vesicular membranes with targeted lysosomal membranes.

In addition I propose a novel gene therapy approach for the treatment of Pompe Disease, an LSD characterized by glycogen accumulation. This approach relies on the AAV-mediated over-expression of the TFEB gene, a master regulator for lysosomal-autophagosomal biogenesis that is able to partially rescue the lysosomal glycogen storage by increasing the functionality of the lysosomal-autophagosomal pathway.

INTRODUCTION

1 LYSOSOME

1.1 General characteristics

The lysosome was discovered in 1959 by Christian De Duve [2] and has since been the subject of intense studies that have clarified the majority of its cellular functions. Lysosomes are organelles delimited by a single membrane and filled with digestive enzymes that are able to degrade molecules and structures into their elementary constituents. Therefore they represent the final destination for many endocytic and autophagic secretion molecules targeted for degradation or recycling. Furthermore lysosomes are involved in various specific cellular pathways such as autophagic degradation of molecules, matrix modelling, pathogen defence and plasma membrane repair via lysosomal exocytosis.

Lysosomes originate from the fusion between endosomes and the Golgi's hydrolytic vesicles. The Golgi's hydrolytic vesicles, also called primary lysosomes, already contain all necessary hydrolases, but its local pH is not sufficiently acidic for their activation. Therefore lysosomal enzymes are activated only after the primary lysosome fuses with endosomes, as the latter carries proton pumps necessary for the acidification of the lumen.

The lysosomal membrane is very important for lysosomal structure and function as it protects cells from hydrolytic lysosomal enzymes. Moreover it is particularly enriched with glycosylated proteins which are important for the transportation of substrates and functional proteins involved in synthetic processes and trafficking.

Although it is often just considered an “enzyme-filled bag”, the lysosome has numerous cellular roles, and its physiological importance is confirmed by the various storage disorders caused by defects in lysosomal biogenesis, or by reduced or absent degradation ability [3]

1.2 Lysosomal membrane structure

Lysosomal membrane constituents were discovered about 20 years ago: they include cholesterol, sphingolipids, a unique phospholipid composition [4], an abundance of carbohydrates [5] and different membrane proteins, which are responsible for maintaining the integrity of the entire organelle. Membrane proteins are highly specialized for different functions; for example proton pumps keep the lumen acceptably acidic, and carrier proteins translocate the products of hydrolytic degradation, such as amino acids, simple sugars and small lipids.

Lysosomal membrane proteins are also involved in fusion with other organelles like autophagosomes, plasma membrane and others lysosomes [6]. The SNARE (Soluble NSF Attachment Protein REceptors) protein family is particularly important for the fusogenic capability of lysosomal membranes as it represents the minimal machinery

required for membrane fusion. SNARE proteins are classified as vesicle SNAREs (v-SNAREs), located on the vesicles membrane, and target SNAREs (t-SNAREs), located on the membranes of target compartments. SNAREs may vary in size and composition, but they all share a 60-70 amino acid cytosolic domain (SNARE motif) that can assemble into *trans*-SNARE complexes. The *trans*-complex, formed by four helical bundles, contains three SNARE proteins: a v-SNARE on one membrane, and two t-SNAREs (in this case one of the t-SNAREs carries two SNARE motifs) on the opposing membrane. The *trans*-SNARE complex interacts with soluble carriers that trigger its ability to mediate membrane fusion by inducing local physical stress on the bilayer. When the membranes fuse, the *trans*-SNARE complex becomes *cis*-SNARE complex, because after fusion, the SNARE proteins are no longer designated to opposing membranes, but instead share the single resulting fused membrane. The components can then de-assemble by way of other soluble factors; at this point each SNARE that was involved in the fusion process is now free from complex and is recycled back to its original compartment to mediate new rounds of fusion.

Experiments with monoclonal and polyclonal antibodies [7, 8] reveal a high content of glycosylated integral proteins, which are enriched both with lysosomes and late endosomes. Such proteins are designated as Lysosome Associated Membranes Proteins (LAMPs), Lysosomal Membranes Glicoproteins (LGPs) and Lysosomal Integral Proteins Membranes (LIMPs).

Given its peculiar composition, the lysosomal membrane covers both structural and functional roles. For one it separates acidic hydrolase from the other cellular

constituents to prevent unwilling degradation. It also mediates different cellular processes such as translocation of substrates targeted for degradation, and even fusion with organelles like autophagosomes, for degradation, or with plasma membrane and others lysosomes [6], for membrane repair.

1.3 Lysosomal content

The lysosomal lumen is densely filled with various hydrolases (phosphatases, nucleases, proteases, polysaccharidases, oligosaccharidases and lipases) responsible for all of the degradative processes of lysosomes. These enzymes are not only limited to the degradation of specific substrates, but are also involved in many lysosome-mediated cellular processes such as bone remodeling, propagation and formation of metastases, antigen presentation, hormone processing and plasma membrane repair.

To date more than 50 lysosomal hydrolases have been identified, but the precise mechanisms behind their roles in cell metabolism are far from being completely understood [9]. Lysosomal hydrolases are active at a pH between 4.5 and 5.0, so the lysosomal lumen is constantly maintained at this acidic pH value as a result of the activity of the proton pumping V-type ATPase. This membrane protein uses metabolic energy in the form of ATP to pump protons in the lysosomal lumen.

Because the activity of the V-ATPase generates a transmembrane voltage, another ion, called a counter-ion, needs to move across the membrane to dissipate this membrane potential. A specific ion transporter moves the counter-ion in or out of the

lysosome; the transporter may render the counter-ion an anion upon influx or a cation after efflux. Several ion transporters have been identified, but there remain other unknown transporters.

1.4 Transport Systems

The lysosome plays a central role in cellular trafficking pathways, being the final destination for macromolecular products of endocytic and biosynthetic pathways. For example the low density lipoprotein (LDL) is quickly interiorized by endosomes and routed to lysosomes after binding with specific receptors on the cellular surface, while acidic hydrolases are synthesized in the ER, modified with Mannose-6-phosphate at the *cis*-Golgi and, finally, transported to lysosomes through the *trans*-Golgi network (TGN) by way of a specific Mannose-6-phosphate receptor (M6PR).

Lysosomes are the central hub linking the different sorting systems. At the plasma membrane, molecules can remain either on the cellular surface or be interiorized into endosomes and routed to lysosomes. Molecules may also travel between plasma membranes and endosomes via the TGN. In addition endosomes allow for them to be recycled back to plasma membrane or sent to lysosomes. All molecular trafficking is regulated by a specific molecular machinery capable of recognizing and directing the molecules to their final destinations [10].

Lysosomes are not only involved in degradation and recycling processes, but also in regulating cellular interaction with the extracellular environment. In fact lysosomes

are involved in a secretory pathway, called lysosomal exocytosis, which plays a major role in different physiological processes such as cellular immune response, bone reabsorption and plasma membrane repair [11-13]. Lysosomal exocytosis requires two sequential steps: in the first step, that is Ca^{2+} independent [14], lysosomes are recruited to the close proximity of the cell surface, while in the second step the pool of pre-docked lysosomes fuse with the plasma membrane in response to Ca^{2+} elevation [11, 12]. Ca^{2+} -dependent lysosomal exocytosis was considered to be limited to specialized secretory cells; however, recent studies indicate that this process occurs in all cell types [11, 15, 16].

Although the main steps of lysosomal exocytosis have been elucidated, little is known about its regulation or its coordination with lysosomal biogenesis.

1.5 Lysosomal biogenesis

The importance of lysosomes in cellular functions and its association with different diseases has led to extensive research on lysosomal biogenesis. Currently there are two models being proposed for lysosomal biogenesis: the maturation model and the vesicular transport model [17, 18].

The maturation model suggests that endosomes, formed by plasma membrane internalization, are transformed into lysosomes by the addition and removal of molecules. According to this model endosomes mature into lysosomes and without endocytosis lysosomes would not be formed.

The vesicular transport model suggests that endosomes, late endosomes and lysosomes are pre-existing structures that communicate by continuous rounds of fusion and fission. It is commonly believed that neither hypothesis can adequately describe lysosome formation, and consequently, a final model will retain elements from both hypotheses.

Recent publications have allowed the identification of a gene network regulating lysosomal biogenesis and function in response to different environmental cues. The first relevant discovery was of a new transcription factor, named TFEB (Transcription Factor EB) [19] that positively regulates the expression of genes involved in lysosomal and autophagosomal biogenesis and function regulation [20]. Specifically in normal conditions TFEB is prevalently cytoplasmic, stress (when more lysosomes and autophagosomes are needed) causes it to translocate to the nucleus where it activates the transcription of lysosomal and autophagosomal related genes. TFEB functions by binding the promoters of regulated genes in a consensus sequence called the CLEAR sequence (and defining the so called “CLEAR network”) [21].

Interestingly TFEB translocation in the nucleus is mediated by different environmental cues; one in particular links autophagy to lysosomal biogenesis in response to nutrient deprivation [22]. TFEB interacts with the nutrient sensor complex mTORC1 on lysosomal membrane, and when nutrient are present, phosphorylation of TFEB by mTORC1 inhibits TFEB activity, while inhibition of mTORC1 by starvation or lysosomal dysfunction causes TFEB dephosphorylation

and nuclear translocation [22].

2 LYSOSOMAL STORAGE DISORDERS

Lysosomal Storage Disorders (LSDs) are a group of about 50 diseases characterized by an accumulation of undegraded molecules inside the lysosome, resulting in the formation of large intracellular vacuoles. They are usually caused by lack of a lysosomal hydrolases, or by lack of its activator or transporter, causing the accumulation of a specific substrate in lysosomes for each disorder type.

LSDs are inherited by autosomal recessive traits, except for Fabry Disease, Hunter Disease (MPSII) and Danon Disease, which are caused by X-linked recessive traits.

The clinical phenotypes are vast, as they can vary for age of onset, severity of symptoms and central nervous system manifestation. In fact many LSDs have three different onset forms: infantile, juvenile and adult.

The severity and progression of a Lysosomal Storage Disorder may vary depending on the type of primary accumulation, the types of cells or tissues that cause accumulation of the substrate, the genetic background or the environmental influence.

It is strongly believed that cells and tissues have certain thresholds of enzymatic activities below which clinical manifestation occurs. This may explain how an infantile form and a juvenile/adult form of the same disease can affect different tissues. For example, the β -galactosidase deficiency, which in the infantile form causes severe brain disease, has no brain involvement in the juvenile form.

LSDs can be classified relating to the altered pathway and substrate accumulation:

- Defects in glycan degradation, the most common group of LSDs, represented by about 30 disorders. It can be divided into four subgroups: defects in degradation of glycoprotein, glycolipid, glycosaminoglycan or glycogen
- Defects in lipid degradation
- Defects in protein degradation
- Defects in lysosomal transporters
- Defects in trafficking

2.1 Multiple Sulfatases Deficiency (MSD)

MSD is a very rare LSD in which all the sulfatases are deficient [23, 24]. Sulfatases are hydrolases that cleave sulfate esters from a wide range of substrates such as glycosaminoglycans (GAGs), sulfolipids, and steroid sulfates [25]. This protein family is represented in most eukaryotes and prokaryotes, with some notable exceptions such as *Saccharomices cerevisiae*. While in prokaryotes sulfatases are involved in sulphur scavenging, in vertebrates they are implicated in the turnover and degradation of sulfated compounds, mostly complex molecules that are hydrolysed in lysosomes in concert with acidic glycosidases. Functional correlation among sulfatases is reflected in a high degree of amino acid sequence similarity along the entire length of the proteins, suggesting that they have evolved from a common ancestral gene [25, 26].

MSD is an autosomal recessive disorder caused by the lack of activity in the Formylglycine Generating Enzyme (FGE), coded for by the SUMF1 gene. The FGE enzyme resides in the Endoplasmic Reticulum (ER) and catalyses the conversion of a specific glycine into formyl-glycine in the active site of all the cellular sulfatases. This is a post-translational modification essential for the activity of the sulfatases.

The inactivation of FGE, due to loss-of-function in the SUMF1 gene, results in an impairment of sulfatases' ability to degrade their specific substrates, leading to the accumulation of different types of macromolecules (especially GAGs) in lysosomes.

MSD is a multi-systemic disease that recapitulates the phenotypes of all the other LSDs due to a deficit in a single sulfatase, and this is especially true for symptoms regarding the central nervous system (CNS). In fact a progressive and massive neuronal and glial death in the CNS of MSD patients and mice models has been reported. This is thought to be due to accumulation of undegraded materials and the subsequent inflammatory response, suggesting that apoptosis is the final pathogenic step in LSDs.

The FGE enzyme, although an ER resident, lacks ER-sorting signals in its sequence, but recently we have demonstrated that its retention in the ER is mediated by the PDI protein, which acts as a chaperone for the FGE enzymatic activity [27]. In addition the FGE enzyme can take part in paracrine signalling when reabsorbed by neighbouring cells [28]. We have also demonstrated that FGE trafficking (retention vs. secretion) is precisely regulated by its interaction with two protein shuttles, ERP44 and ERGIC53, which regulate its movement between the ER and the Golgi

apparatus.

Since MSD recapitulates all the phenotypic manifestations of the LSDs it has been widely used as a model to identify the pathogenic mechanisms leading to cell death in LSDs. In our laboratory we developed a transgenic mouse model for the MSD in which the SUMF1 coding region is broken by the insertion of the β -geo cassette [29]. The MSD mouse model obtained has no sulfatase activity, and the phenotype is as severe and progressive as that observed in human patients.

From a clinical point of view, affected individuals show neurologic deterioration with mental retardation, skeletal anomalies, organomegaly, and ichthyosis. Different types of MSD can be distinguished according to the age of onset: neonatal, late infantile (0 to 2 years), and juvenile (2 to 4 years). Neonatal MSD is the most severe form with a broad range of mucopolysaccharidosis-like symptoms and death within the first year of life. Late-infantile MSD, which includes the majority of cases, resembles late-infantile metachromatic leukodystrophy with progressive loss of mental and motor abilities and skeletal changes. There is also an attenuated form of late-infantile MSD with onset beyond the second year of life. Rare cases of juvenile-onset MSD have been reported with onset of symptoms in late childhood and slower progression [30].

2.2 Mucopolysaccharidosis type IIIA (MPS-IIIA)

Mucopolysaccharidosis type IIIA (MPS-IIIA or Sanfilippo syndrome) belongs to a subgroup of LSDs, called the mucopolysaccharidoses (MPSs), caused by the

deficiency of lysosomal enzymes responsible for the catabolism of GAGs [31]. MPS-III A arises from the congenital loss-of-function of sulfamidase (SGSH), a sulfatase enzyme involved in the stepwise degradation of heparan sulfate (HS). There are three other subtypes of MPS-III (MPS-IIIB, C and D), all of which are caused by deficiencies in different enzymes required for HS catabolism. MPS-III A is the most frequent subtype in some populations and the most common of the MPS disorders [32].

In MPS-III A the CNS is the predominant site of pathology. In fact, although the somatic organs are affected in MPS-III A, the dominant clinical features are neurological dysfunction and neurocognitive decline. As a result, patients experience a wide range of symptoms, including delayed development, mental retardation, rapid loss of social skills and learning ability, disturbed sleep, aggression and hyperactivity [31]. The phenotype of MPS-III A is very complex, and not only due to the intracellular accumulation of undegraded GAGs, but also to their secretion in the extracellular matrix.

There exists a mouse model for the MPS-III A resulting from a natural missense mutation in the SGSH gene with a consequent 3% reduction in the enzymatic activity with respect to WT littermate [33]. MPS-III A mice present the accumulation of heparan sulfate from birth, hyperactivity at the third week of age and aggression from the tenth week of age [34, 35]. The disease progression in mice is very similar to that observed in human patients, so this model is widely used to study the pathogenic mechanisms at the basis of the disease and the effects of different possible therapies.

2.3 Pompe Disease (PD)

Pompe disease is a severe metabolic myopathy caused by the deficiency of acid alpha-glucosidase (GAA) an enzyme responsible for breaking down glycogen to glucose within the acidic environment of lysosomes. The functional deficiency or complete absence of the enzyme results in accumulation of glycogen within this cellular compartment [36, 37]. PD pathology is also characterized by secondary accumulation of autophagic debris (autophagic build-up), typically found in skeletal muscle fibres [38-40].

Even if GAA deficiency is a systemic disorder (distended glycogen-filled lysosomes can be found in multiple tissues) the principal pathological effect of the storage is on skeletal and cardiac muscles.

Pompe Disease has different severity and age-onset in patients: in the most serious infantile form, the disease manifests as profound weakness, hypertrophic cardiomyopathy, heart failure, feeding difficulties, respiratory infections and, if left untreated, causes death within the first year of life. In the attenuated phenotypes, characterized by later (childhood, juvenile or adult) onset, cardiac muscle is usually spared, but the illness remains a serious condition with progressive motor impairment, respiratory failure and premature death [37].

A transgenic mouse model for PD has been generated by knocking-out the GAA gene [41]. GAA $-/-$ mice show different phenotypes at different ages, recapitulating both the infantile and adult form of PD, so they are a useful tool for the study of PD

pathology and therapy. At 3 weeks of age, GAA $-/-$ mice begin to accumulate glycogen in lysosomes due to the lack of GAA activity, and the accumulation increases progressively thereafter. By 3.5 weeks of age, these mice have markedly reduced mobility and strength. However they grow normally, reach adulthood and remain fertile throughout their lives. By 8-9 months of age animals develop obvious muscle wasting and a weak, waddling gait [41].

3 THERAPIES FOR LSDs

Few therapies are available for LSDs, and treatments are mostly symptomatic as they are not able to completely revert the pathologic phenotype. There are different trials and procedures in experimental testing mainly based on enzyme replacement therapy, bone marrow transplantation, ex-vivo and in-vivo gene therapy, enzyme enhancement therapy and substrate reduction.

However the lack of complete knowledge of the pathogenic mechanisms behind the disease is still problematic when developing new therapeutic approaches to the treatment of LSDs.

3.1 Enzyme Replacement Therapy (ERT)

ERT consist of the administration of a recombinant WT form of the lacking enzyme directly into the haematic circulation of LSDs patients. ERT is based on the discovery

that the metabolic defect of cultured fibroblasts from mucopolysaccharidosis patients can be compensated by addition of corrective factors which proved to be the wild type counterparts of the deficient lysosomal enzymes [42]. The added enzymes are rapidly internalized into the lysosomal compartment where they catabolize the accumulated substrates. Importantly only 1-5% of the normal cellular activity was required for correction. The detection of this corrective mechanism led to the optimistic prediction that LSDs should be generally treatable by administration of the respective intact lysosomal enzyme, a treatment strategy designated as enzyme replacement therapy (ERT).

The uptake of lysosomal enzymes into the lysosomal compartment of fibroblasts and other cells depends on receptor-mediated endocytosis via a Mannose 6-phosphate receptor (M6PR). The M6PR binds Mannose-6-phosphate residues (M6P) which are normally added to a sulfatase amino acid chain in the Golgi. M6PR residues play a central role in sorting sulfatases from the Golgi to lysosomes biosynthetically and in their uptake from the extracellular matrix. After binding at the cell's surface, the receptor-ligand complexes cycle from the plasma membrane to an endosomal compartment where the ligands dissociate and reach the lysosome, and contemporarily, the receptors are recycled back to plasma membrane. Due to this peculiar trafficking pathway, ERT is a good candidate for the treatment of all the LSDs caused by a mutation in lysosomal enzymes.

ERT of animal models for various LSDs such as MPS-I [31], MPS-IIIB [43], MPS-VI [44, 45], MPS-VII [46], Fabry disease [47], Niemann-Pick disease [48] and

Pompe disease [49] revealed that intravenously infused lysosomal enzymes are rapidly internalized by liver, spleen and other peripheral tissues, but usually do not enter the brain parenchyma in therapeutically efficient amounts. As a consequence the visceral, but not the CNS, pathology can be improved.

The CNS is not reached by the recombinant enzyme, principally due to the activity of the Blood Brain Barrier (BBB), so several efforts were undertaken to favour the delivery to CNS. Studies in a mouse model of MPS-VII revealed that recombinant β -glucuronidase is able to reach the brain parenchyma when it is injected into newborns whose BBB is still leaky [50]. Two weeks later, however, the BBB is fully differentiated and prevents further uptake of enzyme from the circulation.

Other attempts to overcome the BBB comprise invasive strategy such as intracerebroventricular infusion or temporary disruption of the tight junctions between cerebral endothelial cells, by infusing hypertonic solutions, [51], and non-invasive strategy based on conjugates between blood-brain shuttle vectors and therapeutic enzymes [52, 53]. A recent work demonstrated the efficacy of gene delivery of a modified SGSH for the correction of CNS lesions in MPS-IIIa mice [54]. In this work the authors show that the addition of the blood brain barrier binding domain (BD) from the Apolipoprotein B (ApoB-BD) to the SGSH enzyme is able to mediate the BBB crossing and allow the SGSH to efficiently reach the CNS, resulting in the correction of CNS lesions.

3.2 Bone Marrow Transplantation (BMT)

This approach arises from the idea that a fraction of newly synthesized lysosomal enzymes is not targeted to lysosomes, but instead released from a “producer” cell to be re-absorbed by neighbouring cells [55, 56]. Several experiments demonstrated that the transfer of a therapeutic enzyme from a WT producer cell to an enzyme-deficient cell is able to achieve metabolic correction of the deficient cell in a process called cross-correction.

The discovery of cross-correction allowed the development of a new therapeutic strategy: the supply of a deficient cell is achieved by transplantation of enzyme-producing cells, which transfer the enzyme by a release/uptake mechanism or direct cell-to-cell transfer to neighbouring cells.

In BMT producer cells are bone marrow-derived microglial cells that are able to repopulate the CNS [57-59]. It has been reported that BMT therapy in a cat model of α -mannosidosis, is able to lead to the appearance of α -mannosidase in neurons and other cells of the CNS concomitant with the loss of intracellular storage vacuoles [56]. Treated cats showed little or no progression of neurologic signs 1-2 years post-transplant, whereas untreated cats became severely impaired and reached end-stage disease by 6 months of age.

However, further BMT trials in animal models were less effective in most cases, and no improvement of the brain pathology was detectable, e.g., in a cat model of GM2 gangliosidosis treated by an identical protocol [60].

The variability of therapeutic success may be due to differences of enzyme

production, modification and secretion from producing cells.

Clinical studies for BMT protocol in human patients have been done since 1980, especially for mucopolysaccharidoses, and showed that BMT is able to ameliorate visceral symptoms, such as hepatosplenomegaly, respiratory problems and cardiac function, and might even arrest or slow down neurological deterioration [61, 62].

However as for ERT, the efficacy of BMT is dependent on different factors, such as the age of therapy and the kind of enzyme missing, and even if BMT can have a beneficial effect on visceral symptoms, and to a lesser extent on bone disease, the effect on neurological symptoms varies. Furthermore BMT generally does not result in a normal phenotype and is associated with a mortality rate of 10%, even if an HLA-identical donor is available [63, 64], so the risks and possible benefits of BMT need to be balanced carefully for each individual patient.

3.3 Ex-vivo Gene Therapy

The classical BMT approach can be enhanced by taking advantage of the recent knowledge of cDNA expression and vector packaging systems. In fact donor cells can be genetically modified by *ex vivo* gene therapy prior to transplantation. The rationale for this approach is explained by the elevation of the enzyme production and delivery by constitutive expression of the correcting enzyme from a strong, usually viral promoter. Furthermore *ex vivo* gene therapy allows the use of the patient's own cells as enzyme-producers, thereby eliminating the risk of immune responses to

unmatched donor cells or graft-versus-host disease [65].

The most promising approach in this field is that of hematopoietic stem cell mediated gene therapy. The effects of conventional BMT and bone marrow stem cell gene therapy have been compared in a mouse model of MPS-I [66].

Transplantation of unmodified WT bone marrow was effective in reducing storage in liver and spleen, but not in kidney or brain. Gene therapy using bone marrow overexpressing human α -L-iduronidase from a retroviral vector, however, also corrected the pathology of kidney, choroid plexus, and thalamus. This study clearly supports the notion that bone marrow stem cell gene therapy can be superior to conventional BMT.

In larger animals, including man, retrovirus-based gene therapy is associated with particular problems. Autologous bone marrow from dog models of fucosidosis and MPS-I, which was transduced with retroviral vectors encoding α -fucosidase and α -L-iduronidase, respectively, failed to engraft after transplantation [67, 68]. Indeed authors supply evidence that the non-myeloablated recipients developed a cellular immune response that specifically eliminated transgene-expressing donor-type cells. Unstable engraftment as well as low transduction efficiency was also noticed in a clinical trial analysing the fate of retrovirally transduced autologous CD34+ cells after transplantation into Gaucher patients [69]. Due to these complications, the bases of which are not fully understood, bone marrow stem cell gene therapy has not been successfully applied to larger animals so far.

3.4 In vivo Gene Therapy

The discovery of vector systems, also infecting non-dividing cells, allowed the development of a new kind of therapy, based on the delivery of the WT form of the mutated gene directly *in vivo* [65]. Viral vectors for gene therapy are not able to replicate in cells because they have a defective genome that only carries the genes for infection.

Gene therapy is in theory a good option for all the cases in which the correcting enzyme is not able to reach missing cells due to the lack of internalization signals as observed in some cases of ERT or BMT.

There are different studies using adenovirus, adeno-associated virus or retrovirus vectors as vehicles for gene-transfer into living organisms.

Adenoviruses carry their genetic material in the form of dsDNA and are able to infect both dividing and non-dividing cells. After infection they are not able to integrate their genetic material's content into the genome of the hosting cell. Therefore the transgene expression is only transient and no longer achieved after cell division. For this reason treatment with the adenovirus will require constant re-administration. Adenoviruses are largely used as vectors because their lack of integration into the host cell's genome may prevent the outbreak of unwanted collateral effects, such as cancer. There are different works showing improvements of pathology in visceral organs but not in CNS of mouse models of LSDs after systemic injection of adenoviruses carrying the WT form of the mutated gene [70-73]. Another study

showed that it is possible to achieve a partial restoration of CNS pathology by injecting adenoviral vectors directly into the brain [74].

Adeno-associated viruses (AAVs) are only able to replicate in a cell already infected by an adenovirus since they require adenoviral machinery for replication. AAVs carry their genetic material in the form of dsDNA and are able to infect both dividing and non-dividing cells. Different from adenoviral vectors, AAV vectors can integrate into the host genome, resulting in a more stable transgene expression even if they are principally non-integrating viruses. Low immunogenicity and lack of inflammatory side effects are further advantages of this vector class. Systemic injections of AAV into newborn mice have been reported to be effective for the treatment of both systemic and CNS pathology, even if the major effect on CNS is achieved only by intra-cerebral injections [75].

Retroviral vectors integrate into the host genome but are only able to infect dividing cells. Even if they are not very attractive for gene therapy due to the limitation of infective abilities, retroviruses have been used in therapy because of their large packaging capacity and their integrating property, which can result in a long-term and stable expression of the enzyme. [76, 77].

3.5 Enzyme Enhancement Therapy

This approach exploits the residual activity of the mutant endogenous enzyme in mild phenotypes, for example, those due to misfolding or mutation out of the active site.

In particular two different strategies have been proposed for therapy: the first one utilizes protease inhibitors which may increase the half-life of misfolded, but lysosomally targeted, enzymes by reducing their proteolytic degradation rate [78]. The second one utilizes co-chaperones that are specific small-molecule ligands that bind to the catalytic site of an enzyme and rescue mutant polypeptides by assisting their correct folding in a pre-lysosomal compartment [79].

3.6 Substrate Reduction Therapy

This approach aims to reduce the amount of storage acting on the anabolic pathway rather than the catabolism of substrates, for example with the use of inhibitors for the *de novo* synthesis of substrates [80, 81]. Interestingly a combination between BMT and SRT further prolonged survival, indicating a synergistic effect between the two treatment strategies [82]. Due to good results of knockout mice combination therapy, it might therefore be especially advantageous for early-onset forms of the disease characterized by a very low or absent residual enzyme activity.

4 PATHOGENESIS IN LSDs

Even if primary and secondary storages (not directly related to the missing enzyme) have been largely described and studied, little is known about the effects of storage

on cell vitality and their link to pathogenesis in LSDs. Different theories have been proposed [83]: alterations in lysosomal functionality, intracellular trafficking and signalling or interference with gene expression.

On one hand the accumulation of undegraded material results in the alteration of lysosomal membrane function and structure determining the leakage of lysosomal enzymes into the cytosol. This can lead to the activation of lysosome-mediated apoptotic pathway [84, 85]. On the other hand, lysosomal storage can interfere with the trafficking and sorting functions of lysosomes, thus resulting in the alteration of sub-cellular localization of receptors and enzymes. Furthermore the accumulation of undegraded materials can interfere with the functionality of other cellular pathways determining the secondary accumulation of toxic compounds, as in the case of psicosisin [86].

Moreover cellular storage can interfere with gene expression regulation determining the activation of particular apoptotic genes. For example it has been reported that in the CNS of LSDs with a neurological phenotype, there is an over-activation of pro-inflammatory genes in the microglial compartment with a consequent inflammation-related neuronal death [87-89].

Recently it has been reported that the autophagic pathway plays a pivotal role in mediating cell death and pathology in LSDs. Autophagy is a degradative pathway in which double-membraned organelles (autophagosomes), containing cytoplasmic molecules and organelles, have to fuse with lysosomes for the degradation of their cargoes. Autophagy mediates the degradation of big molecules and maintains the

turnover of cytoplasmic organelles. It is very important for cellular vitality, vertebrate development and immune response.

The autophagic rate is finely regulated in response to different stimuli such as nutrient deprivation, cytoplasm remodelling during embryogenesis, oxidative damage response and prevention of aggregation of toxic molecules in cytoplasm [90-92]. It has been reported that blocking autophagy leads to neurodegeneration in KO mice for autophagic genes [93, 94].

In our laboratory and in other studies, it has been reported that the deactivation of autophagy is due to an alteration in lysosomal fusogenic capability, and leads to the accumulation of toxic aggregates and damaged organelles in the cytoplasm of cells derived from various mouse models of LSDs [95-100].

However little is known about the mechanisms of lysosomal storage that lead to an impediment of the autophagy, even if this is an important point for the treatment of LSDs because the restoration of this particular pathway can be a good target for therapy.

AIM OF THE THESIS

The molecular mechanisms at the basis of cellular and tissue pathology in LSDs are not yet fully characterized. Moreover current therapies, mainly based on the restoration of the enzymatic activity that is lost, are insufficient in completely restoring normal conditions.

The principal aim of this work is then to first identify a pathologic molecular mechanism common to all LSDs and to use the deriving knowledge to develop a new therapeutic approach to LSDs.

In particular in the first part of my work, I studied lysosomal membrane properties and functions in mouse embryonic fibroblast (MEFs) derived from mouse models of MSD and MPS-III A. Specifically I demonstrated that the accumulation of cholesterol in these two LSD models causes an altered organization of the endolysosomal membranes, resulting in the expansion of regions enriched in this lipid. Cholesterol accumulation on lysosomal membrane affects the fusogenic capability of lysosomes by sequestering SNARE proteins in unproductive complexes and impairing their recycling.

In the second part of my work I developed a new therapeutic approach for the treatment of LSDs that circumvents the problem of inefficient enzymatic activity, typical of all classic therapeutic approaches, by exploiting the ability of lysosomes to expel their content into the extracellular space, thus providing clearance of the stored material [101]. Specifically I characterized the effect of TFEB overexpression in a

mouse model of Pompe Disease. Expression of TFEB in myotubes and muscle fibres resulted in lysosomal fusion with plasma membrane, lysosomal exocytosis and a consistent reduction of intra-lysosomal glycogen accumulation. In addition TFEB overexpression in muscle of PD mice alleviated autophagic pathology by promoting the formation and removal of autophagolysosomes.

RESULTS

1 IDENTIFICATION OF THE MOLECULAR PATHOGENIC MECHANISM IN LSDs

1.1 Lysosomal fusion is impaired in LSDs

The trafficking of lysosomes, endosome and autophagosomes is impaired in both MSD and MPS-III A. Figure 1 shows that epidermal growth factor (EGF) stimulation lysosomal-mediated degradation of EGF receptor (EGFR) is more efficient in wild-type (WT) cells than in LSD cells.

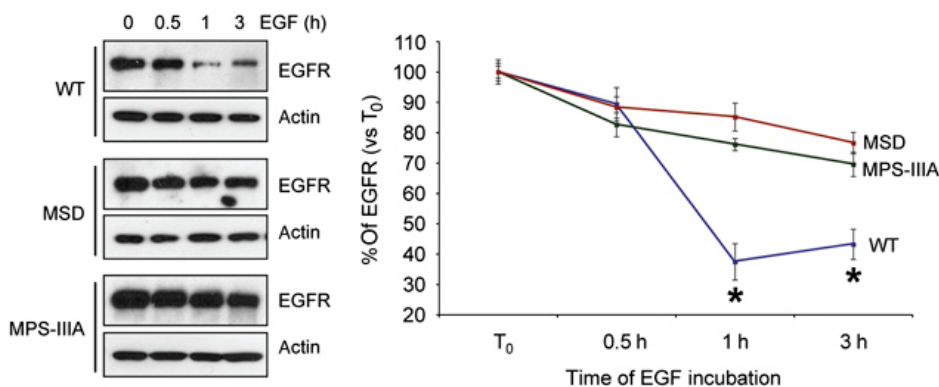


Fig. 1 EGFR degradation is impaired in LSD cells. EGFR degradation was followed in MSD, MPS-III A and WT MEFs by treating the cells with EGF for the indicated time to stimulate EGFR internalization. The cells were immediately lysed and subjected to anti-EGFR blotting. The amount of remaining EGFR was quantified by densitometry analysis (ImageJ) of the blot and expressed in the chart as % of the EGFR amount present at time T₀ (100%). The values in the chart represent the mean \pm s.e.m. values of three independent experiments. *P<0.05, Student's *t*-test: WT versus MSD and WT versus MPS-III A.

We also performed a transport assay by loading cells with a fluorescently labelled dextran, showing that after 6h of chase, the percentage of dextran delivered to lysosomes (as revealed by the co-localization between dextran and the lysosomal marker LAMP1) is significantly higher in WT compared to that in LSD cells (Fig. 2).

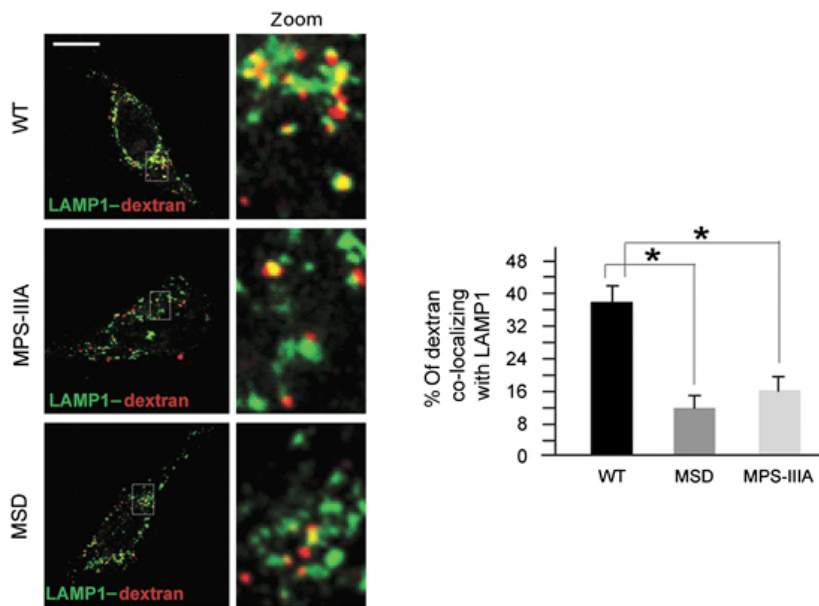


Fig. 2 Dextran uptake is impaired in LSD cells. MSD, MPS-III A and WT MEFs cells loaded with dextran (alexafluor-594-conjugated) were labelled with anti-LAMP1 antibody and the percentage of dextran co-localizing with LAMP1 was evaluated. The chart displays merge values (mean \pm s.e.m.) that represent the percentage of dextran co-localizing with LAMP1 measured in 15 different cells of triplicated experiments. * $P < 0.05$, Student's *t*-test: WT versus MSD and WT versus MPS-III A at each time point. Scale bar: 10 μ m.

Thus indicates that in LSD cells the traffic of membranes to the lysosomal compartment is impaired. We analysed the rate of fusion between lysosomes and autophagosomes using a tandem fluorescent-tagged autophagosomal marker in which LC3 was engineered with both monomeric red fluorescent protein (mRFP) and GFP. In this assay the GFP fluorescence loss is a direct measurement of autophagosome fusion because of GFP quenching by lysosomal acidic pH [1]. The validity of this analysis is not affected by the decreased degradation capability of lysosomes in the

LSD models analysed, as the green fluorescence is rapidly quenched by protonation occurring in the acidic lysosomal lumen (Fig. 3A). Specifically WT and LSD cells were transfected with the mRFP-GFP-LC3 construct, and the autophagosome maturation was followed over a 3h period. The rate of autophagosome maturation was markedly slower in LSD cells compared to that of WT cells (Fig. 3B). All of these findings indicate a decreased delivery of cargo to the lysosomes and an impaired ability of lysosomes to fuse with target membranes in LSD cells.

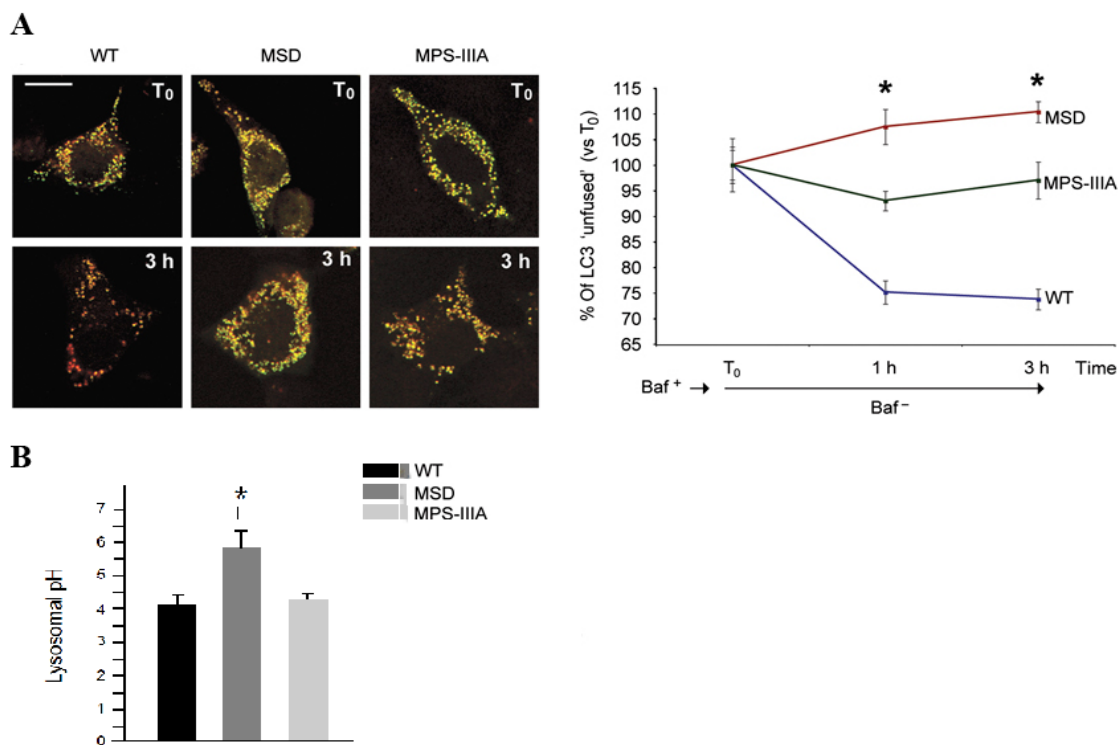


Fig. 3 Lysosomal fusion is impaired in LSD cells. The rate of lysosome fusion with autophagosomes was monitored in MSD, MPS-III A and WT MEFs transfected with a tandem fluorescently tagged LC3 [1]. The rate of autophagosome maturation reflected the percentage of LC3 “unfused” (green/red ratio) at each time (1 and 3 h) after bafilomycin removal (T₀). The percentage of the LC3 “unfused” was displayed versus the value at T₀ (assumed to be 100%). Values are represented as means ± s.e.m of triplicate experiments *P<0.05, Student’s *t*-test: WT versus MSD and WT versus MPS-III A at each time point. Scale bar: 10µm.

1.2 Cholesterol accumulates in the endolysosomal membrane of LSDs reducing

the efficiency of lysosomal fusion

To analyse lysosomal membrane structure and properties, we isolated lysosomes and late endosomes from LSD and WT MEFs using a magnetic chromatography procedure [102]. We observed increased levels of cholesterol in membranes from LSD lysosomes compared to those in WT (Fig. 4A). This is consistent with Filipin staining, showing that cholesterol accumulated inside the endolysosomal vesicles and decorated LAMP1-positive membrane regions (Fig. 4B)

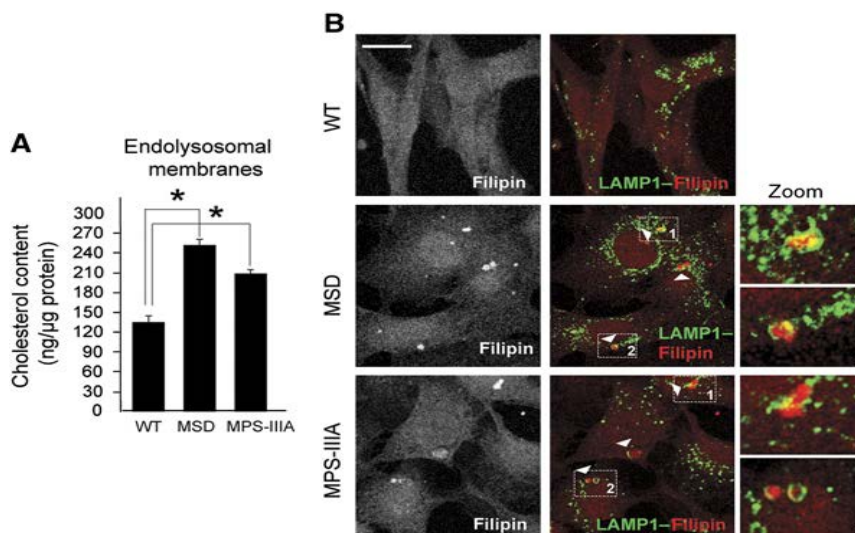


Fig. 4 Cholesterol accumulation in endolysosomal membrane from LSD cells. (A) Cholesterol levels were measured in the indicated endolysosomal membrane samples containing an equal amount of proteins and expressed as ng of cholesterol per μg of protein. Values represent the means ± s.e.m values of three independent experiments * $P < 0.05$, Student's *t*-test: WT versus MSD and WT versus MPS-III A. **(B)** Filipin staining showing cholesterol accumulation in the endolysosomal compartment of MSD and MPS-III A MEFs (Arrowheads and enlarged images). Scale bar, 10 μm **(B)**

Importantly no significant changes in the bulk of phospholipids were observed, with the exception of an increase in lysobisphosphatidic acid (LBPA) (Fig. 5A and B).

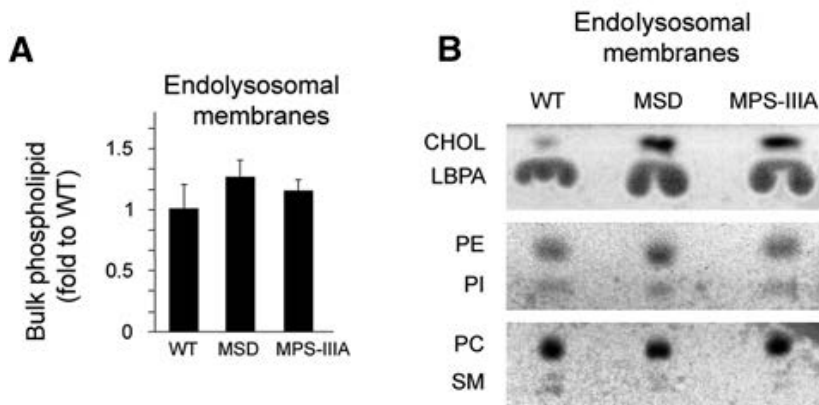


Fig. 5 Alteration in lipid composition of endolysosomal membranes from LSD cells. (A, B) Total lipids extracted from the indicated endolysosomal membrane sample (30 μ g of proteins) were either (A) subjected to a phosphate assay to quantify the bulk of phospholipids or (B) separated by TLC. Phospholipids and cholesterol on TLC plates were revealed by molybdenum blue staining. CHOL, cholesterol; LBPA lysobisphosphatidic acid; PC, phosphatidylcholine; PE phosphatidylethanolamine; PI phosphatidylinositol; SM, sphingomyelin.

We tested the effect of cholesterol accumulation on lysosomal fusogenic capability by modulating cholesterol level in the endolysosomal membranes from WT and LSD cells and then monitoring lysosomal fusion efficiency. Specifically we achieved cholesterol overloading on lysosomal membranes of WT cells by treatment with methyl- β -cyclodextrin (M β CD)-complexed cholesterol (Fig. 6A), while we achieved cholesterol depletion from lysosomal membranes of LSD cells by the treatment with M β CD (Fig. 6B).

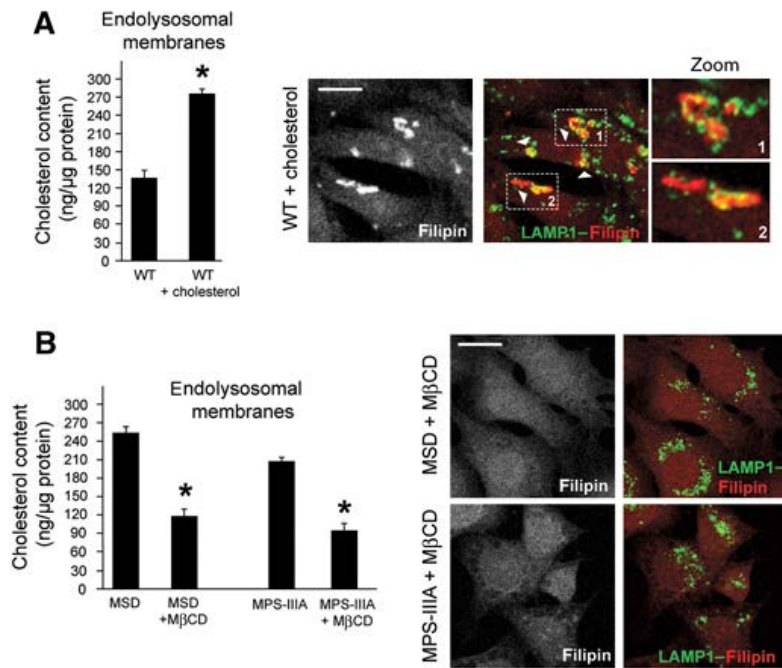


Fig. 6 Cholesterol modulation in LSD and WT cells. Endolysosomal membrane cholesterol measurements and Filipin staining were carried out in either (A) WT MEFs loaded with cholesterol or in (B) MSD and MPS-III A MEFs treated with MβCD. Arrowheads and enlarged images show cholesterol accumulation in endolysosomes of cholesterol-loaded WT MEFs. Values are represented as means ± s.e.m of triplicate experiments *P<0.05, Student's *t*-test: (A) WT versus WT+cholesterol; (B) MSD versus MSD+MβCD and MPS-III A versus MPS-III A+MβCD. Scale bar, 10 μm (A,B).

Cholesterol overloading in WT cells resulted in a decreased rate of both autophagosome maturation (Fig. 7A) and lysosomal endocytic transport (Fig. 8A), and conversely, cholesterol depletion in LSD cells resulted in a normalization of both autophagosome maturation (Fig. 7B) and lysosomal endocytic transport (Fig. 8B). These findings indicate that abnormal cholesterol levels in the endolysosomal membrane directly affect the ability of lysosomes to efficiently fuse with target membranes in the cells.

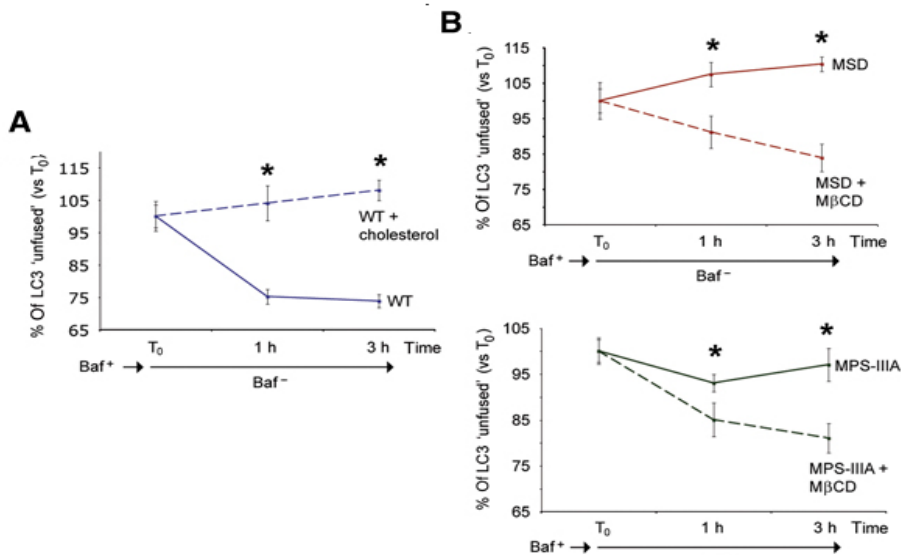


Fig. 7 Cholesterol accumulation inhibits lysosomal/autophagosomal fusion. WT MEFs were overloaded with cholesterol (A) while MSD and MPS-III A were treated with MβCD (B). After treatments the rate of autophagosome maturation were also analysed as in Figure 1. Values are represented as means ± s.e.m of triplicate experiments *P<0.05, Student's *t*-test: (A) WT versus WT+cholesterol; (B) MSD versus MSD+MβCD and MPS-III A versus MPS-III A+MβCD.

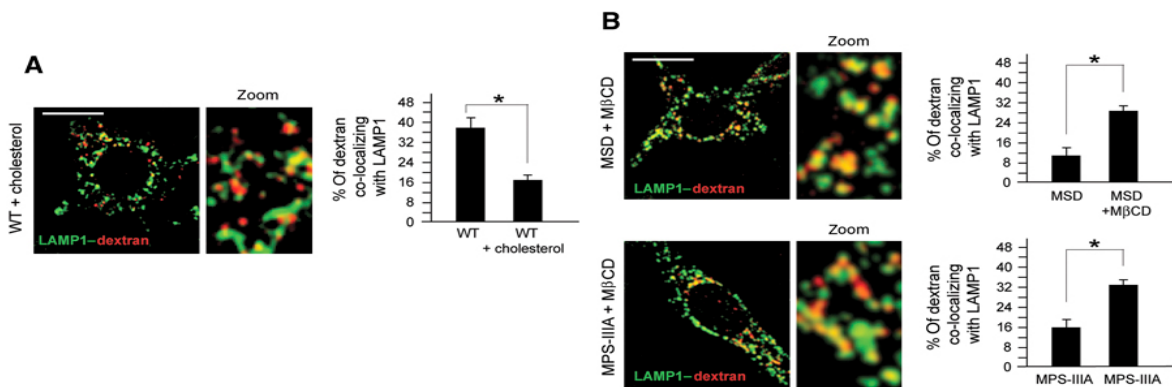


Fig. 8 Cholesterol accumulation inhibits lysosomal/endosomal fusion. WT MEFs were overloaded with cholesterol (A) while MSD and MPS-III A were treated with MβCD (B). After treatments the transport of dextran to lysosomes was also analysed as in Figure 2. Values are represented as means ± s.e.m of triplicate experiments. *P<0.05, Student's *t*-test: (A) WT versus WT+cholesterol; (B) MSD versus MSD+MβCD and MPS-III A versus MPS-III A+MβCD. Scale bar, 10 μm (A, B).

1.3 The organization of the endolysosomal membranes is altered in LSD cells

Biological membranes have a peculiar structural organization in which cholesterol plays various roles. For example it increases lateral heterogeneity and determines the segregation of a subset of lipids and proteins into ordered domains which are enriched with cholesterol and glycosphingolipids. It has been proposed that these membrane domains constitute discrete entities termed “lipid rafts”, which mediate important function in membrane signalling and trafficking [103-106]. The components of these cholesterol-enriched regions are resistant to detergents, thus allowing for biochemical coalescence into an insoluble fraction, termed detergent-resistant membranes (DRMs), which can be isolated after centrifugation in a sucrose gradient [107] and identified by Flotillin-1 immunostaining.

The analysis of DRMs in endolysosomal membranes of LSD and WT cells showed an increase in the percentage of Flotillin-1 associated with DRMs of LSD cells (Fig. 9), indicating an increased amount of cholesterol-enriched regions in these endolysosomal membrane samples.

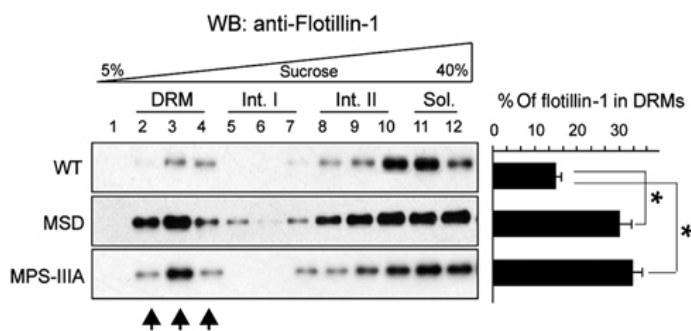


Fig. 9 LSD endolysosomal membrane contains increased amount of detergent resistant domains (DRMs). Endolysosomal membranes from MSD, MPS-III A and WT MEFs were treated with 1% Triton X-114 and loaded on a sucrose gradient. Immunoblots with Flotillin-1 identified DRMs in fractions 2, 3 and 4 (arrows). The fractions at the bottom of the gradient (12 and 13) correspond to high-density detergent soluble fractions, whereas the remaining ones were defined as intermediate fractions (intermediate-I: 5, 6, 7 8; intermediate-II: 9, 10 and 11). The percentage of Flotillin-1 in DRMs was calculated from the densitometric quantification of immunoblots. Values are represented as means \pm s.e.m of triplicate experiments. * $P < 0.05$, Student's *t*-test: WT versus MSD and WT versus MPS-III A.

This was also supported by immuno-electron microscopy (EM) analysis, which showed an accumulation of the glycosphingolipid GM-1, a component of cholesterol-enriched membrane domains in the membranes of LSD endolysosomes (Fig. 10).

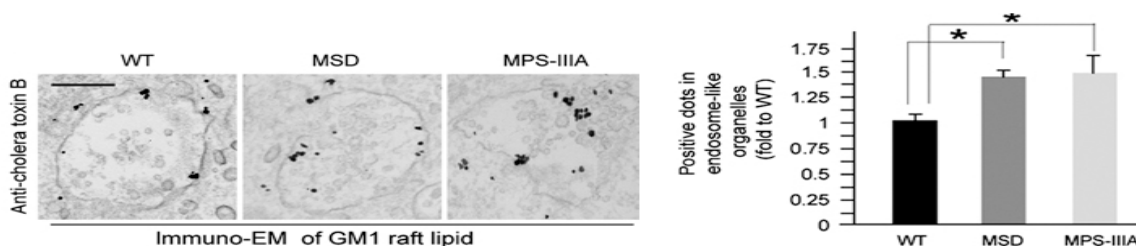


Fig. 10 The LSD endolysosomal membrane contains increased amount of cholesterol-enriched regions. Immuno-EM of GM1 lipid was carried out in WT, MSD and MPS-III A MEFs by staining cells with anti-cholera toxin B antibodies (see Materials and methods section). The number of GM1-positive dots was measured in 25 cells from three independent experiments and displayed as fold to WT. Values are represented as means \pm s.e.m of triplicate experiments. * $P < 0.05$, Student's *t*-test: WT versus MSD and WT versus MPS-III A. Scale bar, 0.3 μ m.

We also measured membrane order of the isolated membranes using the fluorescent probe C-laurdan [108]. Notably, despite the overall increase in DRMs and GM1 levels, LSD endolysosomal membranes maintain a membrane order that is similar to that observed in WT cells (Fig. 11). This may be due to a general and proportional build-up of both raft and non-raft membrane regions, and is consistent with previous reports of an expansion of the endolysosomal compartment in LSD cells [109].

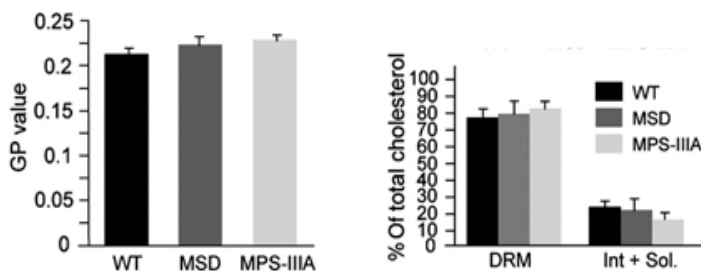


Fig. 11 The LSD endolysosomal membranes maintain a membrane order similar to WT endolysosomal membranes. Endolysosomal membranes from MSD, MPS-III A and WT MEFs were stained with C-laurdan and subsequently analyzed by fluorescence spectrophotometry to calculate the GP value (see Materials and methods section for details). Distribution of cholesterol was also measured throughout the gradient and expressed as percentage of total cholesterol in raft (DRMs) and soluble fractions. Values are represented as means \pm s.e.m of triplicate experiments. * $P < 0.05$, Student's *t*-test: WT versus MSD and WT versus MPS-III A

Cholesterol changes on LSD endolysosomal membranes is associated with an increase in the amount of DRM-associated proteins and a decrease in the amount of proteins present in the soluble regions of the gradient with respect to the protein distribution observed in control samples (Fig. 12). This aberrant protein compartmentalization is restored by M β CD treatment, which leads to a reduction of DRM fraction (Fig. 12).

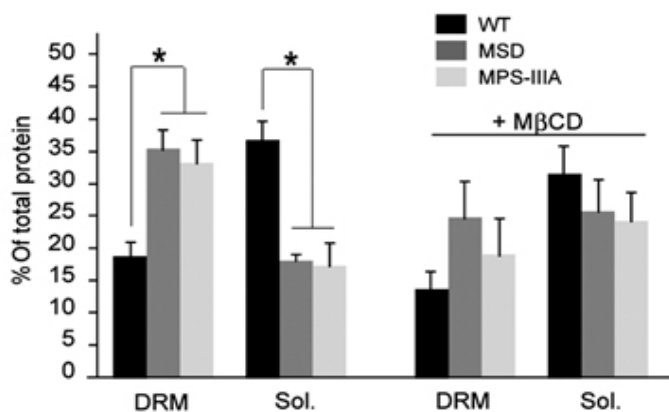


Fig. 12 LSD endolysosomal membranes show an abnormal protein content in LSD cells. Equal aliquots from either DRMs or soluble fractions were pooled, the protein content determined and displayed as percentage of total protein in DRM and soluble gradient regions. Values are represented as means \pm s.e.m of triplicate experiments. * $P < 0.05$, Student's *t*-test: WT versus MSD and WT versus MPS-III A for each fraction.

The increase of DRM proteins is specific for a peculiar sub-set of proteins, as demonstrated by a similar distribution profile of the transferrin receptor in WT and LSD cells, that is normally excluded from DRMs, and the distribution of LAMP1, which has a more linear distribution across the gradient (Fig. 13). Our results suggest a cholesterol-mediated reorganization of a subset of endolysosomal membrane proteins.

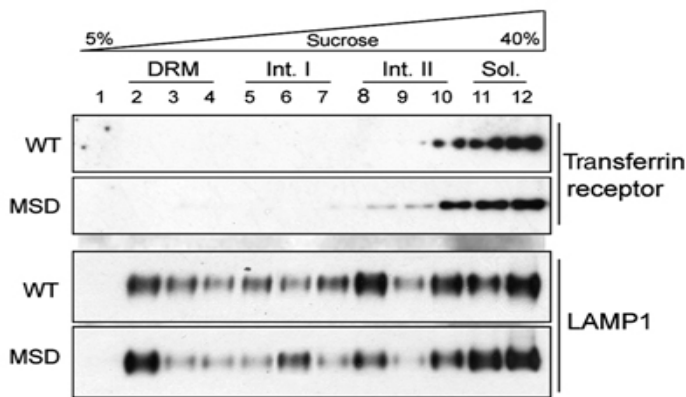


Fig. 13 Protein distribution on endolysosomal membranes is altered in LSD cells. Immunoblotting profiles of the transferrin receptor and LAMP1 in the sucrose gradient.

1.4 Endolysosomal SNARE membrane compartmentalization is highly dependent on cholesterol and is altered in LSD cells

SNAREs are transmembrane proteins that drive membrane fusion in endocytic pathways by assembling into high-affinity *trans*-complexes between two opposing membranes [110, 111]. Previous studies have demonstrated that plasma membrane SNAREs are functionally organized into clusters, the integrity of which is dependent on cholesterol [112-116]. To elucidate the effect of membrane cholesterol abnormalities observed in LSD endolysosomes on SNAREs functionality, we analysed the lysosomal membrane distribution of VAMP7, Vti1b and syntaxin 7, which are post-Golgi SNAREs belonging to differential combinatorial set of SNAREs. These post-Golgi SNAREs participate in *trans*-complexes and drive the fusion of endolysosomal membranes with either endosomes or autophagosomes [117]. Our results shows that these SNAREs become detergent-resistant in LSD cells, as we observed that VAMP7, Vti1b and syntaxin 7 are more associated with DRM

regions at the expense of the SNARE content present in the soluble region of the gradient (Fig. 14A and B). This SNARE redistribution across the endolysosomal membrane is cholesterol-dependent as demonstrated by cholesterol depleting or loading, respectively, in LSD and WT cells. Treatment of LSD cells with M β CD resulted in the dissociation of SNAREs from the DRMs, restoring a SNARE distribution similar to that observed in WT cells (Fig. 14A and B). Conversely, loading WT cells with cholesterol resulted in an increased association of SNAREs with DRM regions, thus mimicking the conditions observed in LSD cells (Fig. 14A and B).

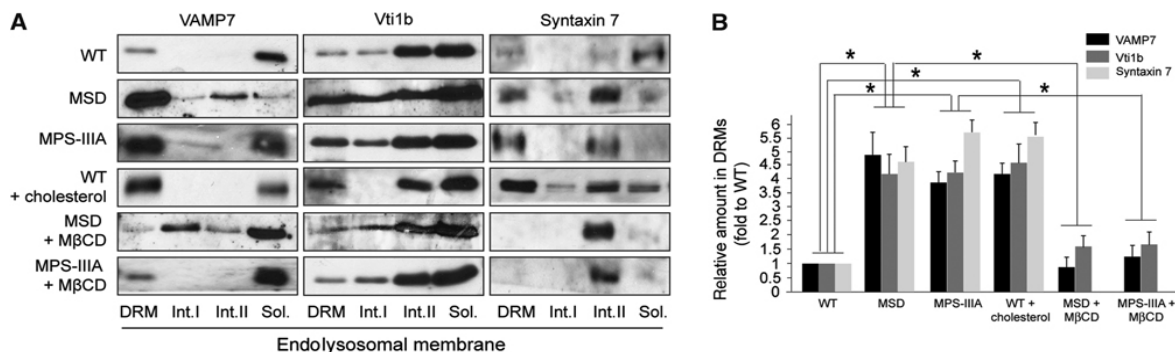


Fig. 14 SNAREs are sequestered by cholesterol within endolysosomal membranes. (A) VAMP7, Vti1b and syntaxin 7 distributions in endolysosomal membranes from MSD, MPSIII A and WT MEFs were evaluated by immunoblotting analysis of gradient fractions. To simplify the analysis the DRM, the intermediate-I, the intermediate-II and soluble fractions of the gradient were pooled separately and then subjected to immunoblotting. SNARE distribution was also analyzed after loading WT cells with cholesterol and after M β CD treatment. In MSD and MPSIII A MEFs, all analyzed SNAREs abnormally accumulate in DRMs of lysosomal membranes. Cholesterol modulation results in a change of SNARE distribution. (B) The percentage of each analyzed SNARE observed in DRM fractions was quantified from blots (ImageJ densitometry analysis) and displayed as relative amount versus WT. Values are represented as means \pm s.e.m of triplicate experiments. *P<0.05, Student's *t*-test: WT versus MSD, WT versus MPS-III A, WT versus WT+cholesterol, MSD versus MSD+M β CD, MPS-III A versus MPS_III A+M β CD for each analysed SNARE.

These findings were associated with a remarkable enrichment of VAMP7, Vti1b and

syntaxin 7 in the endolysosomal membranes of both cholesterol-loaded and LSD cells, which was significantly higher compared with that observed for LAMP1 (Fig. 15 and Fig. 16), the distribution of which was not affected by DRM and was similar in WT and LSD cells (Fig. 13).

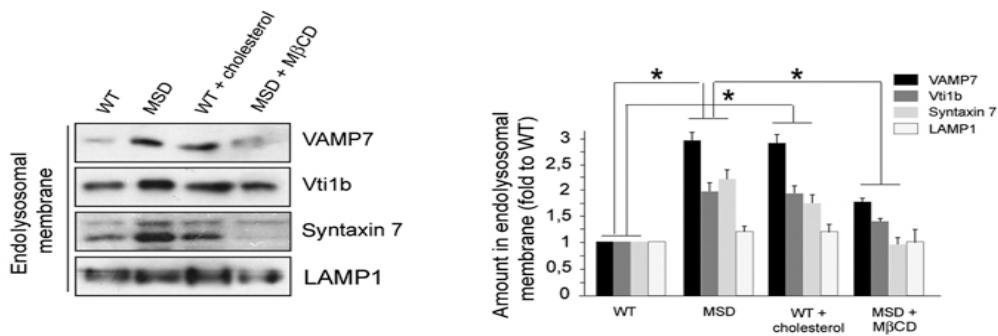


Fig. 15 SNARE proteins are overexpressed on endolysosomal membranes of cholesterol-loaded cells. Immunoblots and relative quantification showing SNARE protein levels along with LAMP1 protein levels in endolysosomal membranes from WT (untreated and cholesterol treated) and MSD MEFs (untreated and MβCD treated). In the graphs, the protein levels were displayed as relative amount versus WT. Values are represented as means ± s.e.m of triplicate experiments. *P<0.05, Student's *t*-test: WT versus MSD, WT versus WT+cholesterol and MSD versus MSD+MβCD for each analysed protein.

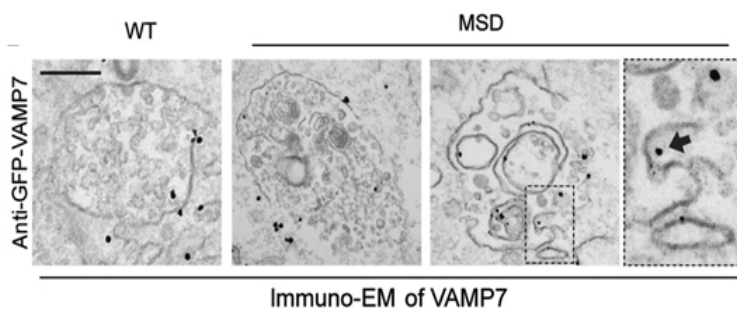


Fig. 16 VAMP7 distribution is affected in LSD cells. WT and MSD MEFs transfected with GFP-VAMP7 were stained with anti-GFP for immuno-EM. The enlarged image shows internalization of GFP-VAMP7 particles (arrow). Scale bar, 0.3 μm.

However we observed a limited increase in the amount of the analysed SNAREs in total cell lysates (Fig. 17) whereas LAMP1 showed a more significant increase (Fig.

17), consistent with the expansion of the endolysosomal compartment in LSD cells.

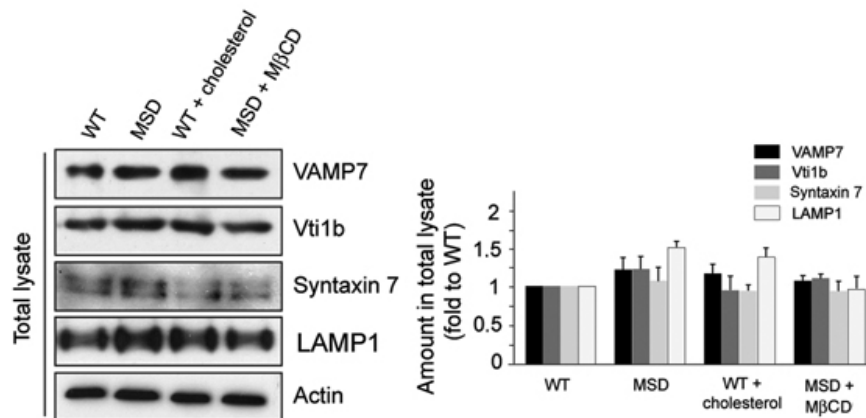


Fig. 17 SNARE proteins are overexpressed in cholesterol-loaded cells. Immunoblots and relative quantification showing SNARE protein levels along with LAMP1 protein levels in total lysates from WT (untreated and cholesterol treated) and MSD MEFs (untreated and MβCD treated). In the graphs, the protein levels were displayed as relative amount versus WT. Values are represented as means \pm s.e.m of triplicate experiments. * $P < 0.05$, Student's *t*-test: WT versus MSD, WT versus WT+cholesterol and MSD versus MSD+MβCD for each analysed protein.

This suggests that SNARE accumulation in endolysosomal membranes is the result of an increased cholesterol-mediated sequestration in specific membrane regions, rather than that of slower degradation kinetics due to the reduced degradation capacity of lysosomes in LSDs. Importantly we observed no evidence of altered membrane compartmentalization of the non-lysosomal SNAP23 and Sec22/syntaxin 5 SNAREs that showed a similar distribution in WT and LSD cells (Fig. 18A). Moreover, distribution abnormalities of cholesterol-dependent lysosomal membranes affected SNARE proteins specifically and did not affect other crucial membrane components of the traffic apparatus, as shown by the normal distribution observed for Rab7 (Fig. 18B), a well-established regulator of endocytic membrane trafficking [118].

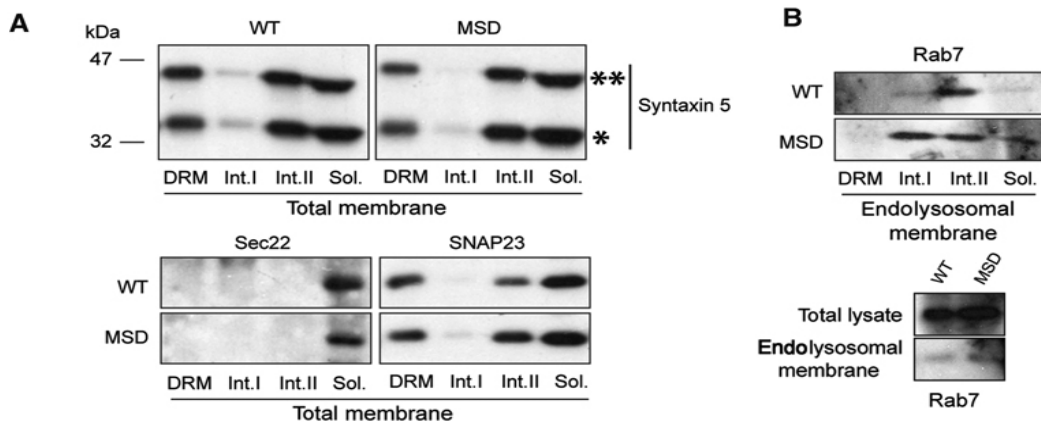


Fig. 18 Association with DRM is specific for SNARE proteins in LSD cells. Syntaxin 5, Sec22 and SNAP23 distribution in total membrane derived from control WT and MSD MEFs. Syntaxin 5 immunoblot shows two bands (*, 35 kDa and **, 42 kDa) corresponding to the two isoforms of the protein. (G) Distribution profile of Rab7 in WT and MSD lysosomal membranes. Values are represented as means \pm s.e.m of triplicate experiments.

1.5 Endolysosomal SNAREs are locked in assembled complexes in LSD cells

The function of SNARE requires an ordered dynamic interaction between different SNAREs with consecutive rounds of assembly, membrane fusion and disassembly of post-fusion SNARE *cis*-complexes [111]. Moreover to maintain membrane identity and ensure new fusion events, post-fusion SNAREs must be trafficked and recycled back to steady-state membrane locations by interacting with specific adaptors of the clathrin vesicular transport [119-122]. We investigated the effect of abnormal SNARE accumulation in DRM of LSD endolysosomal membranes on these dynamic interactions, and thus on SNARE functions.

We first analysed the ability of SNAREs to undergo a correct assembly-disassembly reaction. The amount of assembled SNARE complexes was determined by measuring SNARE complexes levels in boiled and non-boiled SDS treated samples. We found an increase in the amount of SDS-resistant complexes in LSD cells compared with

that in WT and an increased association of these complexes in DRM fractions, as revealed by immunoblot against Vti1b (Fig. 19).

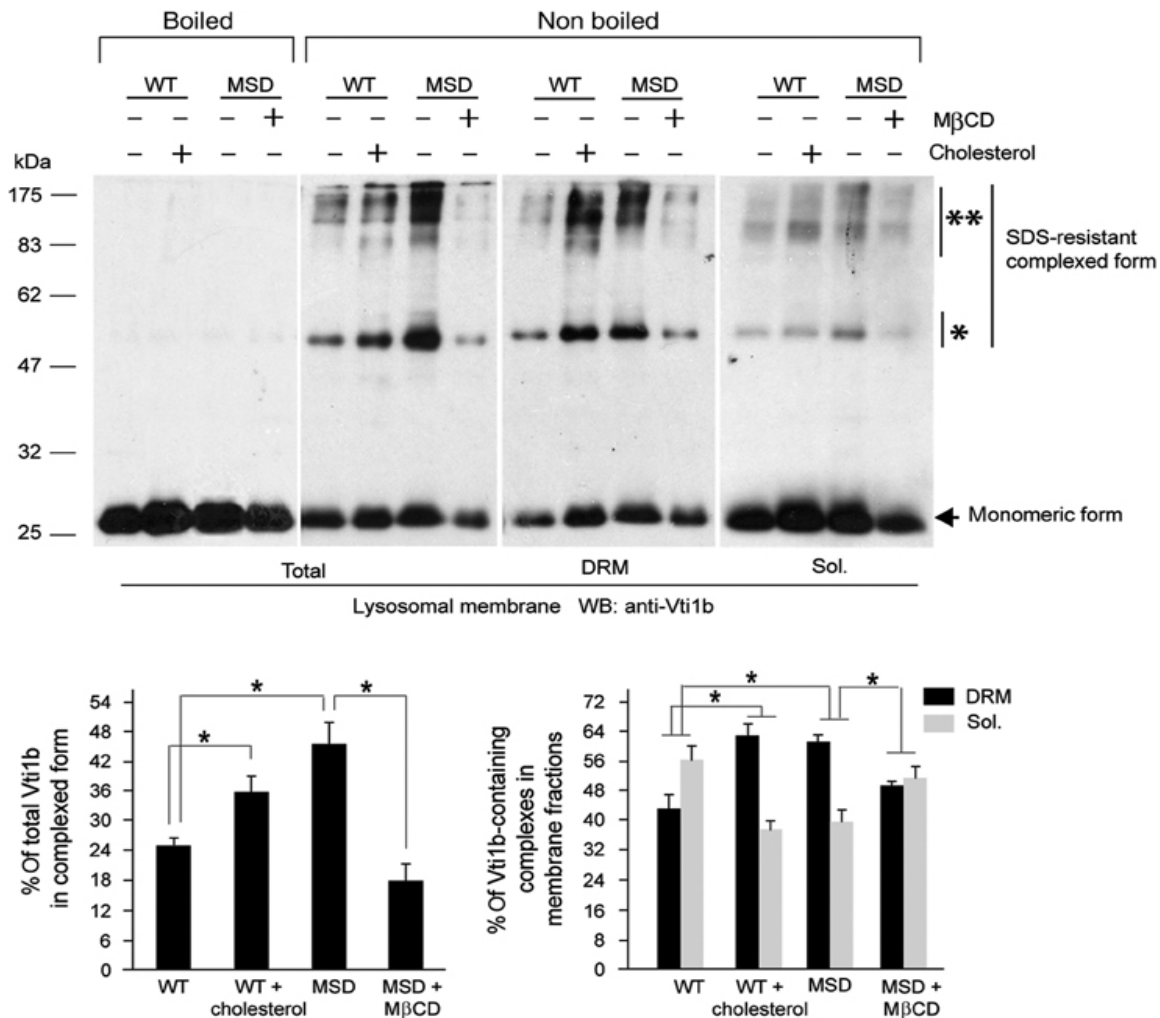


Fig. 19 SNAREs are locked in high molecular weight complexes in LSD endolysosomal membranes. SDS-resistant complexes containing Vti1b were detected by immunoblotting analysis of non-boiled samples corresponding to total, detergent insoluble (DRM) and detergent soluble (Sol.) endo-lysosomal membrane fractions derived from MSD and WT MEFs. The SDS-resistant complexes were also visualized after loading WT MEFs with cholesterol and after treating MSD MEFs with MβCD. Immunoblots revealed the presence of low molecular weight complexes (*, 50–60 kDa) and high molecular weight complexes (**, 480 kDa). The percentage of Vti1b in SDS-resistant complexes in total endolysosomal membranes (bottom-left chart) and the amount of Vti1b-containing SDS-resistant complexes in DRM and soluble fractions (bottom-right chart) were calculated by the densitometric quantification of the correspondent immunoblots (ImageJ). Values represent the mean ± s.e.m. values of three independent measurements. *P<0.05, Student’s t-test: WT versus MSD, WT versus WT+cholesterol and MSD versus MSD+MβCD (bottom-left chart); WT versus MSD, WT versus WT+cholesterol and MSD versus MSD+MβCD for each fraction (bottom-right chart).

These data were confirmed by the increase in the amount of co-immunoprecipitation of syntaxin 7 and VAMP7 with Vti1b in LSD cells with respect to WT cells (Fig. 20).

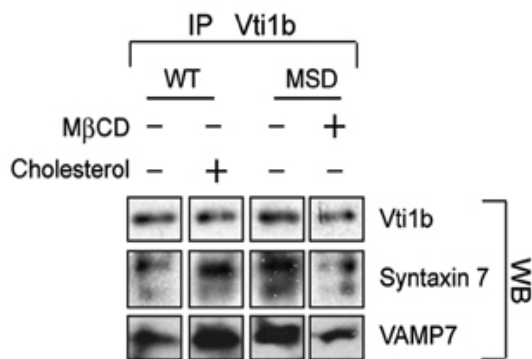


Fig. 20 Snare proteins are locked in assembled form in LSD endolysosomal membranes
 Syntaxin 7 and VAMP7 were co-immunoprecipitated with Vti1b using anti-Vti1b antibodies in WT (untreated or cholesterol treated) and in MSD (not treated or MβCD treated) MEFs. The amount of Vti1b precipitated in each cell line is also shown.

The abnormal distribution of endolysosomal SNARE complexes in LSD cells was rescued by cholesterol depletion, whereas cholesterol loading in WT cells resulted in the formation of abnormal complexes (Fig.19 and Fig. 20). The blotting profile of SDS-resistant complexes indicated the accumulation of both lower and higher molecular weight complexes that were also decorated by the Vti1b cognate SNARE syntaxin 7 (Fig. 21). These complexes may represent, respectively, SNARE dimers and oligomer/fully assembled *cis*-complexes, or alternatively may reflect nonspecific pairing of SNAREs due to their local enrichment in cholesterol membrane microdomains. There was also the evidence of the accumulation of SNARE homodimers containing either Vti1b or syntaxin 7, as shown by the shift of the main band present in the lower molecular weight complexes in the syntaxin blot (Fig. 21).

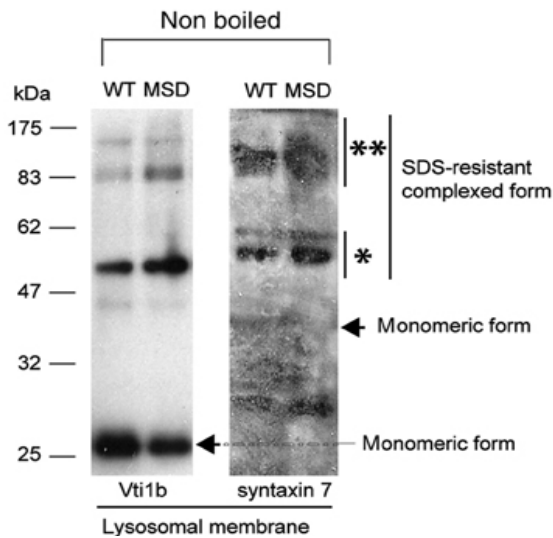


Fig. 21 SNARE complexes in LSD cells are associated to DRMs. SDS-resistant complexes are decorated by anti-syntaxin 7 antibodies in total endolysosomal membrane fraction from WT and MSD MEFs

The α -SNAP adaptor is essential for the recruitment of N-ethylmaleimide-sensitive factor (NSF) on assembled *cis*-complexes for the post-fusion complex disassembly [123, 124]. In addition the NSF-SNAP system has been demonstrated to operate also on some off-pathway SNARE complexes and on SNARE-assembling intermediate complexes [125-127]. We observed that the accumulation of SNARE complexes in both cholesterol-loaded and LSD cells was associated with a mislocalization of α -SNAP that resulted more associated with intracellular membrane than with cytosol (Fig. 22). Moreover this mislocalization was rescued by cholesterol depletion from LSD endolysosomal membranes (Fig. 22). This suggested that the SNARE complexes accumulating in cholesterol-loaded and LSD cells could represent “dead-end”/intermediate or post-fusion complexes undergoing inefficient or partial disassembly.

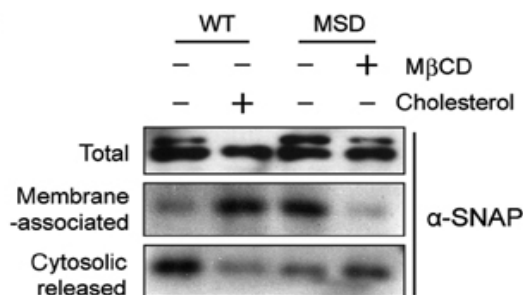


Fig. 22 α -SNAP is more associated with endolysosomal membrane in LSD cells. Membrane-associated α -SNAP and its release in the cytosol were evaluated by western blot analysis on total cell lysates, intracellular membranes recovered after centrifugation from a post-nuclear supernatant fraction (membrane associated) and cell lysates devoid of membranes (cytosolic released) derived from MSD (untreated or M β CD treated) and WT (untreated or cholesterol treated) MEFs.

These findings demonstrate an abnormal cholesterol-dependent accumulation of SNARE complexes in the endolysosomal membranes of LSD cells and indicate an imbalance in the SNARE assembly-disassembly functional cycle.

1.6 The traffic and recycling of post-Golgi endolysosomal SNAREs is inhibited in LSD cells

The sorting and recycling of post-fusion SNAREs is mediated by specific interaction with dedicated clathrin adaptors. Co-immunofluorescence analysis showed an increased co-localization between VAMP7 and Vti1b in LSD cells compared to WT (Fig. 23). Moreover this co-localization took place mostly in LAMP1-positive structures (white merge in Fig. 23), suggesting that SNARE clustering is associated with trapping the lysosomes in LSD cells.

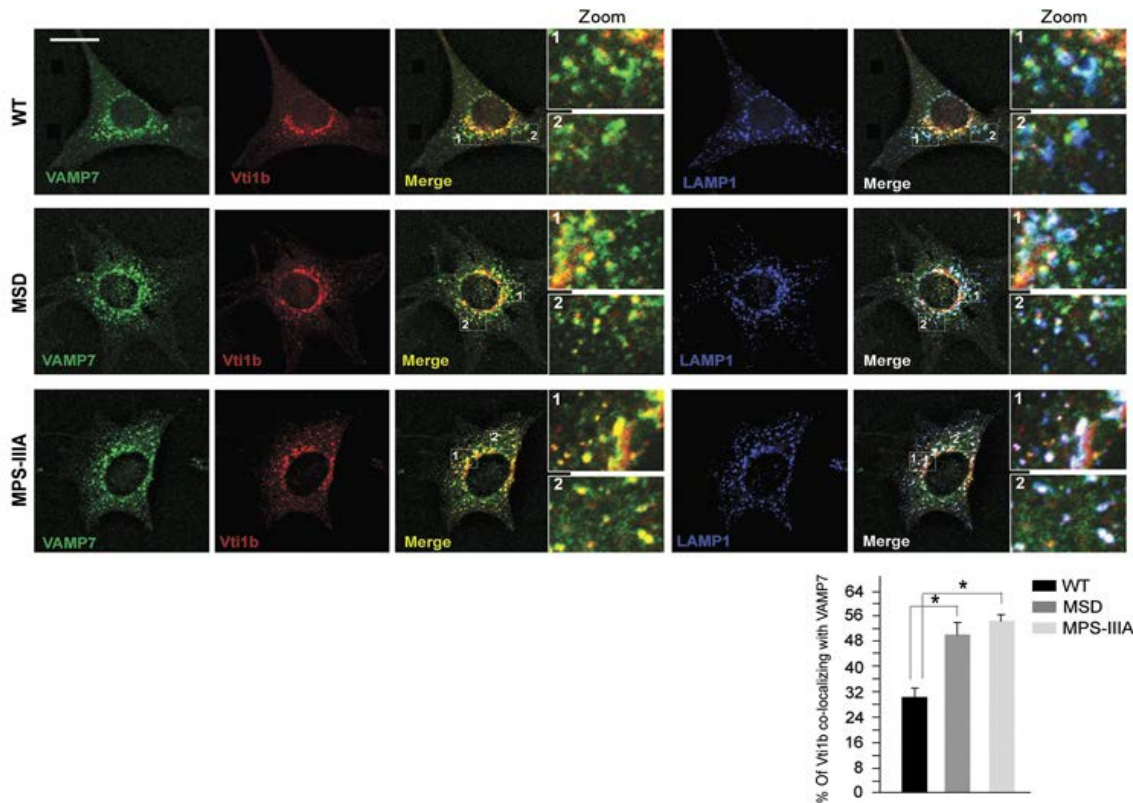


Fig. 23 Increased co-localization of SNARE proteins in LSD cells. MSD, MPS-III A and WT MEFs were subjected to a triple labelling with anti-VAMP7, anti-Vti1b and anti-LAMP1 antibodies. The merges between VAMP7 and Vti1b (double merges in yellow) and between VAMP7, Vti1b and LAMP1 (triple merges in white) are shown (see also enlarged images showing the extent of co-localization in different regions of the cells). The VAMP7–Vti1b co-localization was quantified in 15 different cells and displayed as % of Vti1b co-localizing with VAMP7 (means \pm s.e.m.). * $P < 0.05$, Student's t-test: WT versus MSD and WT versus MPSIII A. Scale bar: 10 μ m.

In normal conditions Vti1b is transported from a late endosomal compartment back to an earlier compartment and/or the *trans*-Golgi network (TGN) through the clathrin adaptor EpsinR [119, 121]. We examined the effect of accumulation of SNARE-complexes in endolysosomal membranes of LSD cells on Vti1b interaction with EpsinR and found a marked decrease of Vti1b co-localization with EpsinR in LSD and cholesterol-overloaded cells (Fig. 24). However the Vti1b overlap with EpsinR increased in LSD cells depleted of cholesterol (Fig. 24).

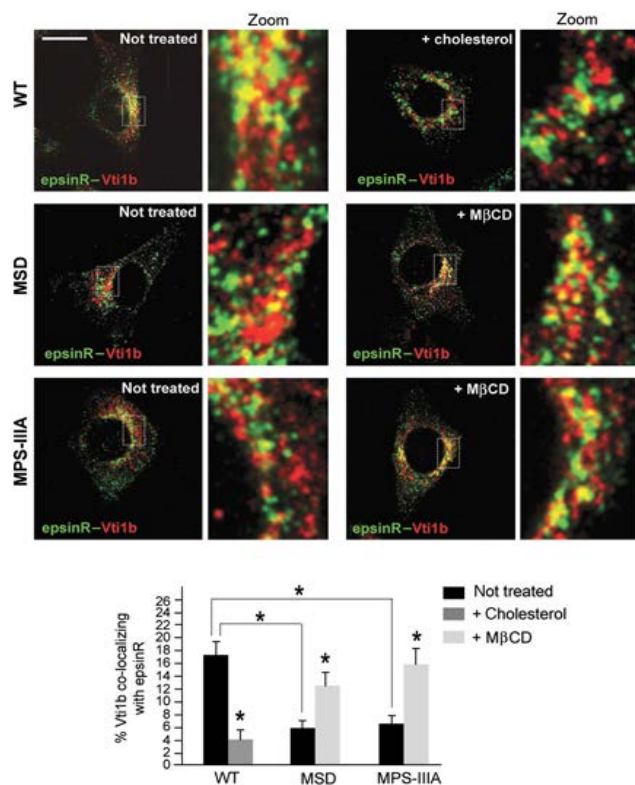


Fig. 24 Cholesterol levels affect SNARE localization. Co-localization of Vti1b with EpsinR was quantified by double-labeling experiments in MSD and MPS-III A (untreated and MβCD treated) and in control WT (untreated and cholesterol treated) MEFs. The chart displays merge values (means ± s.e.m.) that represent the percentage of Vti1b co-localizing with EpsinR measured in 15 different cells. *P < 0.05, Student's t-test: WT versus MSD, WT versus MPS-III A, WT versus WT+cholesterol, MSD versus MSD+MβCD and MPS-III A versus MPSIII A+MβCD). Scale bar: 10 μm.

We confirmed the effect of cholesterol abnormalities in endolysosomal membranes of LSD cells on Vti1b recycling by following the dynamics of Vti1b trafficking route to the TGN in live cells using fluorescence recovery after photobleaching (FRAP) experiments. The fluorescence of transfected GFP-tagged Vti1b (GFP-Vti1b) was photo-bleached in a TGN juxta-nuclear region, and its recovery was tracked for 120-180s. The recovery of GFP-Vti1b fluorescence was faster in WT cells than observed in LSD cells (Fig. 25), indicating an impairment in the Vti1b transport from endolysosomal compartment towards the TGN in LSD cells due to the reduced

interaction with the EpsinR transporter. Interestingly cholesterol depletion in LSD cells was able to increase the mobility of Vti1b (Fig. 25), whereas cholesterol overloading in WT cells resulted in a slowed Vti1b FRAP-kinetics, similar to that observed in LSD cells (Fig. 25). These results demonstrate that the sorting and vesicular transport of post-Golgi SNAREs are impaired in LSD cells due to cholesterol-dependent SNARE clustering that affects SNARE interaction with clathrin adaptors.

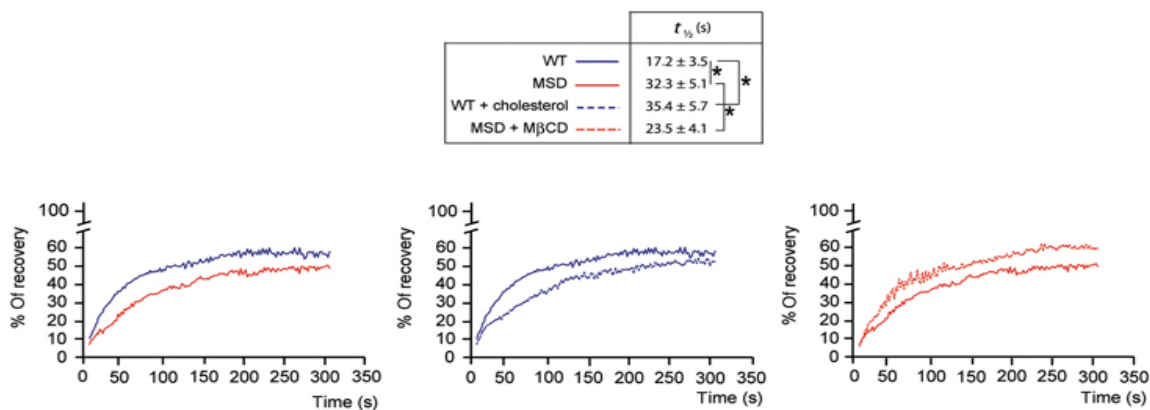


Fig. 25 Cholesterol levels affect SNARE trafficking. Vti1b trafficking was monitored by FRAP analysis in WT (untreated and cholesterol treated) and MSD (untreated and M β CD treated). MEFs transfected with GFP-Vti1b (see Materials and methods section for details). FRAP data are displayed as percentage of recovery with respect to the fluorescence before bleach (100%) and are representative of 10 recordings from different cells. A summary of $t_{1/2}$ values is also shown. * $P < 0.05$, Student's t-test: WT versus MSD, WT versus WT+cholesterol, MSD versus MSD+M β CD.

2 LINKING THE MOLECULAR PHENOTYPE TO THE TREATMENT FOR LSD

The identification of this important pathological mechanism in LSD allowed us to develop new therapeutic approaches for the treatment of LSD. We took advantage of our lab's recent identification of a transcription factor (TFEB), that is the master

regulator of lysosomal and autophagosomal compartment biogenesis [19-21]. In particular we demonstrated that TFEB overexpression is able to positively regulate the expression and function of genes involved in lysosomal and autophagosomal compartment biogenesis. In addition we also demonstrated that TFEB overexpression is able to modulate cellular clearance in LSD cells by increasing lysosomal docking to plasma membrane and exocytosis [101].

So if the principal pathological mechanism is storage build-up in cells leading to lysosomal dysfunction, our hypothesis was to utilize TFEB overexpression to increase lysosomal and autophagosomal functions, and in particular, their exocytosis to mediate cellular clearance. We tested our hypothesis in both an *in vitro* and *in vivo* model of Pompe Disease (PD).

2.1 TFEB overexpression reduces lysosomal size and glycogen burden in PD myotubes

To verify if TFEB can promote lysosomal exocytosis and rescue lysosomal glycogen storage, PD myotubes isolated from the GAA ^{-/-} mouse were infected with an adenovirus vector expressing Flag-TFEB (Ad-TFEB), and were then fixed and immunostained with the lysosomal marker anti-Lamp1 and anti-Flag antibodies.

After 42-78 h post-infection cells showed a robust overexpression, and nuclear staining of TFEB resulting in a dramatic reduction of lysosomal size (Fig. 26A and B). PD myotubes infected with the adenovirus vector (Ad-null) showed large

LAMP1-positive lysosomes similar to those in non-infected PD cells (Fig. 26A).

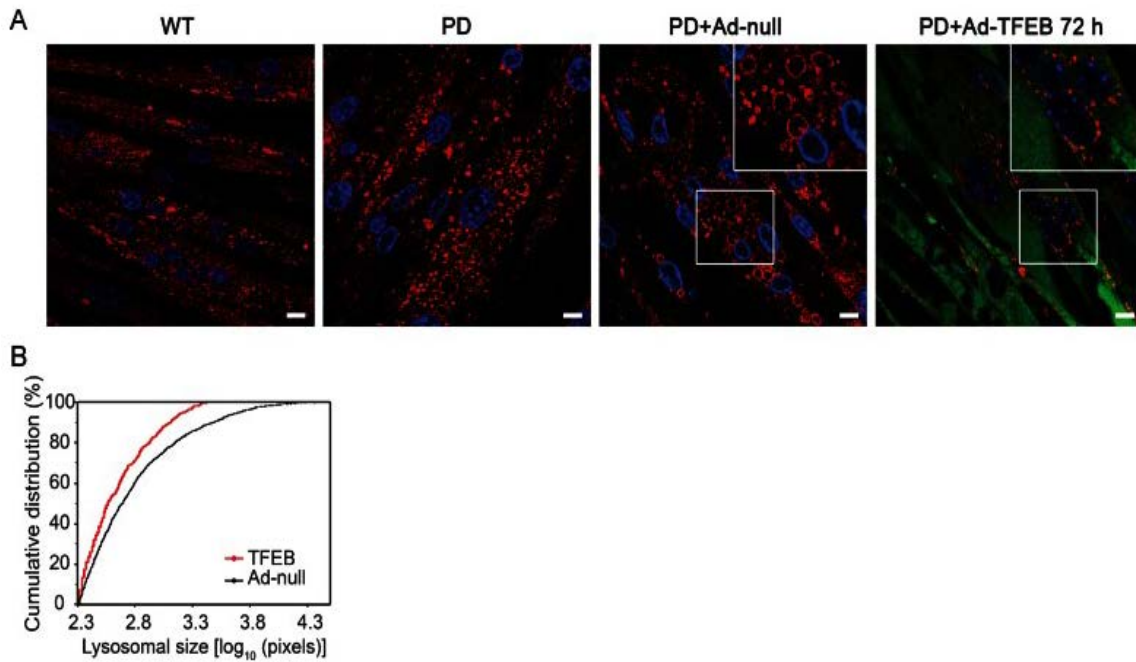


Fig. 26 TFEB stimulates clearance of enlarged lysosomes in PD myotubes. (A) Confocal microscopy image of PD myotubes (cl. 3LE8) infected for 72 h with adenovirus containing TFEB (PD+Ad-TFEB 72 h) shows a dramatic reduction in the number of large LAMP1-positive lysosomes (red) compared to that in untreated (PD) or adenovirus (PD+Ad-null)-treated PD myotubes. WT myotubes are shown on the left panel. Nuclei are stained with Hoechst (blue). TFEB was detected with anti-Flag antibody (green). (B) Distribution of lysosomal size differs significantly in Ad-null and Ad-TFEB PD myotubes ($p=6.32 \times 10^{-8}$; Kolmogorov-Smirnov test). Lysosomal size is expressed as number of pixels representing lysosomal area (LAMP1-positive structures). The median lysosomal size of Ad-TFEB infected myotubes ($m=367.13$ pixels, $n=703$, range 208–2659) was significantly lower than that of Ad-null infected myotubes ($m=491.16$ pixels, $n=1395$, range 200–2857; $p=6.5 \times 10^{-12}$; Wilcoxon rank sum test). Bar: 10 μm .

At 24h post-infection cells showed a relocation of enlarged lysosomes toward the plasma membrane (fig. 27) that is an indication of rapid lysosomal exocytosis.

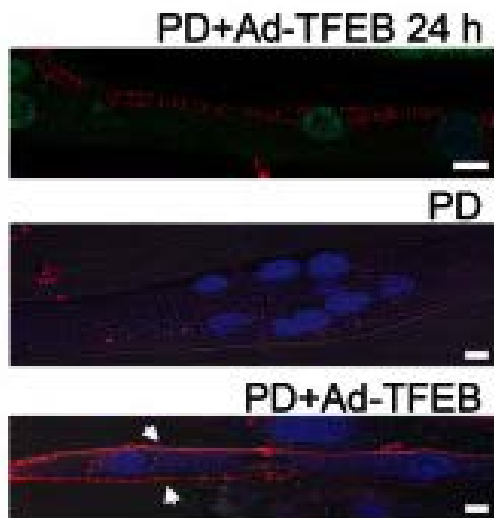


Fig. 27 TFEB induces relocation of lysosomes to the plasma membrane in PD myotubes. Confocal microscopy image of PD myotubes infected for 24 h with Ad-TFEB shows relocation of lysosomes to the plasma membrane (top). Images showing LAMP1 staining (red) on plasma membrane in a PD myotube infected with Ad-TFEB (bottom; arrows) but not in a non-infected cell (middle). Non-permeabilized cells were incubated with anti-LAMP1 antibody at 48C for 40 min, followed by fixation and staining with secondary antibody. Bar: 10 μ m.

In addition we tested the effect of constitutively active mutant TFEB (S211A; TFEBmt) [22, 128, 129] in PD myotubes. Massive accumulation of TFEB in the nuclei resulted in a striking clearance of large lysosomes without any decrease in the total amount of LAMP1 protein (Fig. 29A and B). In fact levels of LAMP1 appear to increase in TFEBmt-treated cells, consistently with the observed role of TFEB in stimulating lysosomal biogenesis [19, 21].

The reduction of enlarged lysosomes in TFEB-treated PD myotubes was associated with a significant decrease in the amount of accumulated storage material as shown by the incorporation of the fluorescent glucose derivative 2-NBDG in glycogen (Fig. 28).

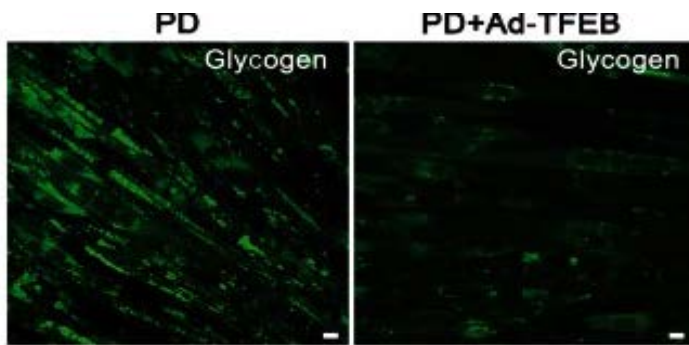


Fig. 28 TFEB reduces glycogen burden in PD myotubes. Confocal microscopy images of live non-infected PD myotubes (left) or PD myotubes infected for 72 h with Ad-TFEB (right) show a dramatic reduction in the amount of accumulated glycogen in TFEB-treated cells. The cells were incubated with the fluorescent glucose (2-NBDG; green), extensively washed, and analyzed using confocal microscopy. Bar: 10 μ m.

These data demonstrate the effectiveness of TFEB overexpression in the reduction of glycogen storages in PD myotubes.

Notably TFEB-overexpressing fibres change their morphology; normally elongated myotubes become spindle-like and contain centrally located nuclei (Fig. 29). However no toxicity was observed, as TUNEL assay revealed only occasional apoptotic cells, and no activation of caspase-3 was detected by western blot in the same treated fibres (Fig. 30).

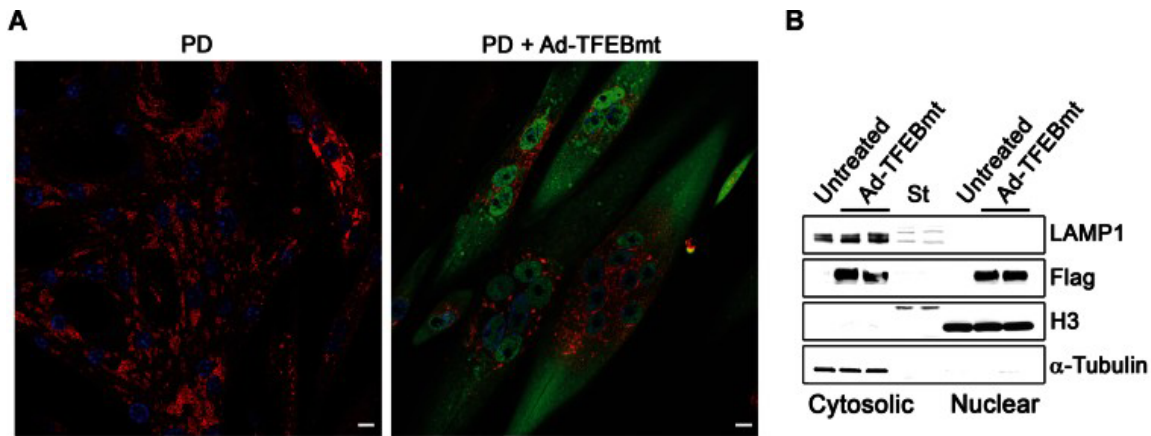


Fig. 29 TFEBmt reduces lysosomal size in PD myotubes. (A) Immunostaining of non-infected cells (day 13 in differentiation medium) and cells infected with a mutant form of TFEB (TFEBmt) with LAMP1 (red) and Flag (green). Ad-TFEBmt was added to the myotubes for 72 h on day 10 in differentiation medium. Ad-TFEBmt-infected cells show massive accumulation of TFEB in the nuclei and significant reduction in lysosomal size, similar to that seen with TFEB. (B) Western blot of cell lysates confirms the presence of TFEB in the nuclear fraction; the different intensities of the two bands corresponding to LAMP1 protein in untreated and TFEBmt-treated samples may reflect the differences in the glycosylation pattern. Bar: 10 μ m.

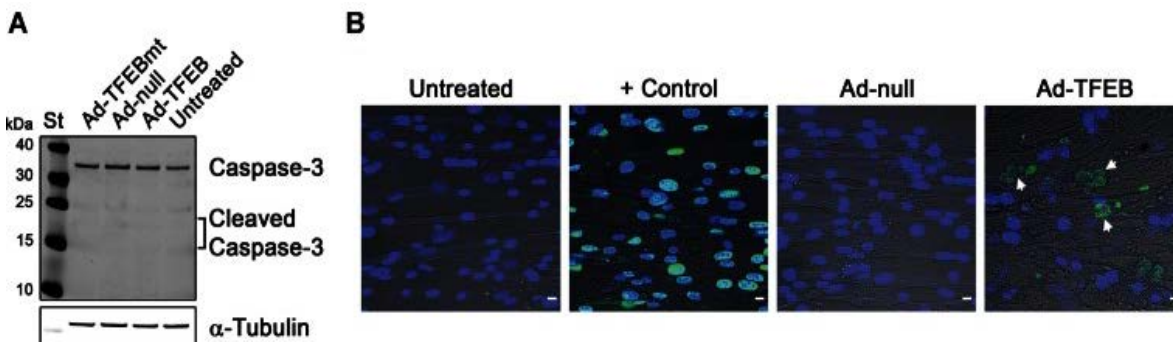


Fig. 30 TFEBmt induces apoptosis in a subset of PD myotubes. (A) Western blot of protein lysates from untreated, Ad-null, TFEB, and TFEBmt-treated myotubes with anti-caspase-3 antibody. No activated (cleaved) products are detected in any condition. α -Tubulin was used as a loading control. (B) TUNEL assay shows the presence of some apoptotic cells in Ad-TFEB-infected cultures, but not in control cultures infected with adenovirus alone (n=3). Bar: 10 μ m.

2.2 TFEB overexpression in PD muscle induces cellular clearance by promoting lysosomal/autophagosomal exocytosis

To evaluate the effect of TFEB on lysosomal and autophagic pathologies *in vivo*, three knockout mouse strains were used: the previously described GAA $-/-$ and autophagy deficient GAA $-/-$ (Atg7:GAA DKO) models [41], and a newly developed GFP-LC3:GAA $-/-$ strain. Flexor digitorum brevis (FDB) muscles from each model were transfected using electroporation with plasmids containing TFEB and/or LAMP1 (Table 1), and live single fibres were analysed four to six days after transfection by time-lapse confocal microscopy, or alternatively, live fibres were fixed and stained for imaging.

Table 1. Experimental design^a

Condition	Mouse strain	Plasmids	Rationale
1 ($n^b = 73$)	GFP-LC3:GAA $-/-$	mCherry-LAMP1	To address lysosomal-autophagosomal interactions; control for conditions 2 & 3
2 ($n = 63$)	GFP-LC3:GAA $-/-$	Flag-TFEB/mCherry-LAMP1	To investigate the effect of TFEB on lysosomal-autophagosomal clearance
3 ($n = 45$)	GAA $-/-$	GFP-TFEB/mCherry-LAMP1	To study TFEB's effect on lysosomal clearance; control for condition 4
4 ($n = 55$)	Atg7:GAA DKO	GFP-TFEB/mCherry-LAMP1	To study the effect of autophagy on TFEB-induced lysosomal clearance
5 ($n = 29$)	Atg7:GAA DKO	mCherry-LAMP1	Control for condition 4
6 ($n = 5$)	GFP-LC3:WT	mCherry-LAMP1	WT control
7 ($n = 47$)	GAA $-/-$	GFP-TFEB	To label mitochondria and lysosomes in live and fixed fibres

^a3-4 animals were used for conditions 1-6; 2 animals were used for condition 7. For each animal ~1000 fibres were isolated.

^b n = number of fibres analysed by confocal microscopy.

Both Flag-TFEB/mCherry-Lamp1 and GFP-TFEB/mCherry-Lamp1-transfected PD fibres showed a striking decrease in the number of large lysosomes, docking and fusion of enlarged lysosomes to the plasma membrane, the emergence of multiple normal dot-like size lysosomes (Fig. 31 and 32) and a markedly increased motility and fusion of lysosomes (Fig. 33) compared to untreated PD controls.

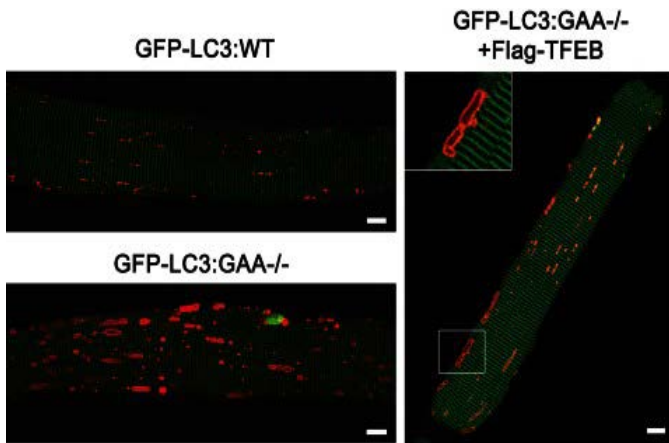


Fig. 31 TFEB promotes clearance of enlarged lysosomes in PD fibres. Confocal microscopy images of live fibres derived from 3 to 4 month-old GFP-LC3: WT (top left), untreated GFP-LC3:GAA^{-/-} (bottom left) or TFEB-treated GFP-LC3:GAA^{-/-} (right) mice. All fibres were transfected with mCherry-LAMP1 to visualize lysosomes (red). The effects of TFEB are clearly visible – overall reduction in lysosomal size, appearance of normal size lysosomes (similar to those in the WT), and lysosomal docking to the plasma membrane (inset). Bar: 10 μ m.

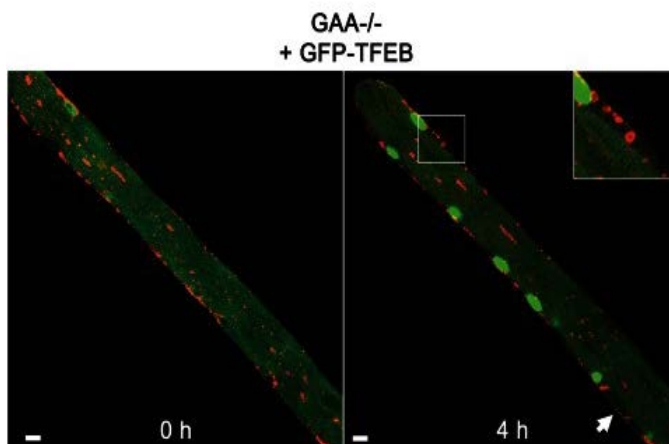


Fig. 32 TFEB induces lysosomal localization to plasma membrane in PD fibres. FDB muscle of a GAA^{-/-} mouse was transfected with both GFP-TFEB and mCherry-LAMP1 (GAA^{-/-} + GFP-TFEB). Images were taken before (left) and after 4 h (right) of time-lapse microscopy. Lysosomal clearance is visible in the TFEB-transfected fibre at both time points. Lysosomes appear to “exit” the fibre (inset and arrow) at the 4 h time point when TFEB is activated, as evidenced by its nuclear translocation (green nuclei). Bar: 10 μ m.

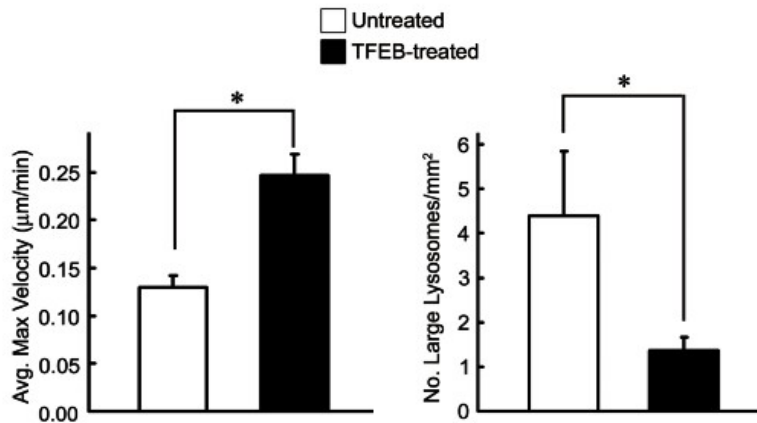


Fig. 33 TFEB increases lysosomal motility in PD fibres. The mean maximum velocity of lysosomes (top) and the number of large (>3.5 µm) lysosomes (bottom) in untreated and TFEB-treated PD fibres (note: all data for Flag- and GFP-TFEB-treated fibres are pooled). Lysosomal velocities were calculated from time-lapse images using ImageJ software with the manual tracking plug-in. For each condition the trajectories of multiple lysosomes were followed (n=26 untreated; n=43 TFEB-treated) and the three highest velocity measurements per lysosome were recorded. In TFEB-treated fibres, the maximum velocity of lysosomes was significantly increased ($p=2.07 \times 10^{-17}$) and the number of large lysosomes was significantly decreased ($p=1.0 \times 10^{-3}$). Ten untreated and 24 TFEB-treated fibres were analyzed for the size calculations. * indicates statistically significant differences ($p \leq 0.001$; Student's t-test). Error bars represent 95% confidence intervals.

Importantly TFEB-transfected fibres showed normal shape and appearance, suggesting that overexpression of TFEB does not cause any appreciable muscle damage.

The use of GFP-LC3:GAA $-/-$ strain revealed the lysosomal/autophagosomal fusion rate as a possible issue causing autophagic build-up. The expression of mCherry-LAMP1 was seen almost exclusively in fibres or region of fibres free of autophagic build-up (80-90% of all transfected fibres), suggesting a compromised lysosomal biogenesis in areas of autophagic accumulation. However in those fibres in which mCherry-LAMP1 was expressed in the build-up area (10-20 %), lysosomal-autophagosomal fusion appear rare or non-existent (data not shown).

It was reasonable to assume that TFEB overexpression may increase lysosomal-

autophagosomal fusion, which would thus prevent or resolve autophagic build-up in PD muscle. To analyse the effects of TFEB on lysosomal-autophagosomal fusion we performed time-lapse microscopy on live GFP-LC3:GAA ^{-/-} fibres transfected with both TFEB and LAMP. We observed an increased co-localization between LAMP1 (red) and LC3 (green) in TFEB treated fibres (Fig. 34A and B) and a clear alignment of doubly labelled autophagolysosomes along the plasma membrane (Fig. 34B). This suggests that TFEB may induce lysosomal/autophagosomal exocytosis. These data raised the intriguing possibility that autophagy may facilitate TFEB-induced lysosomal clearance.

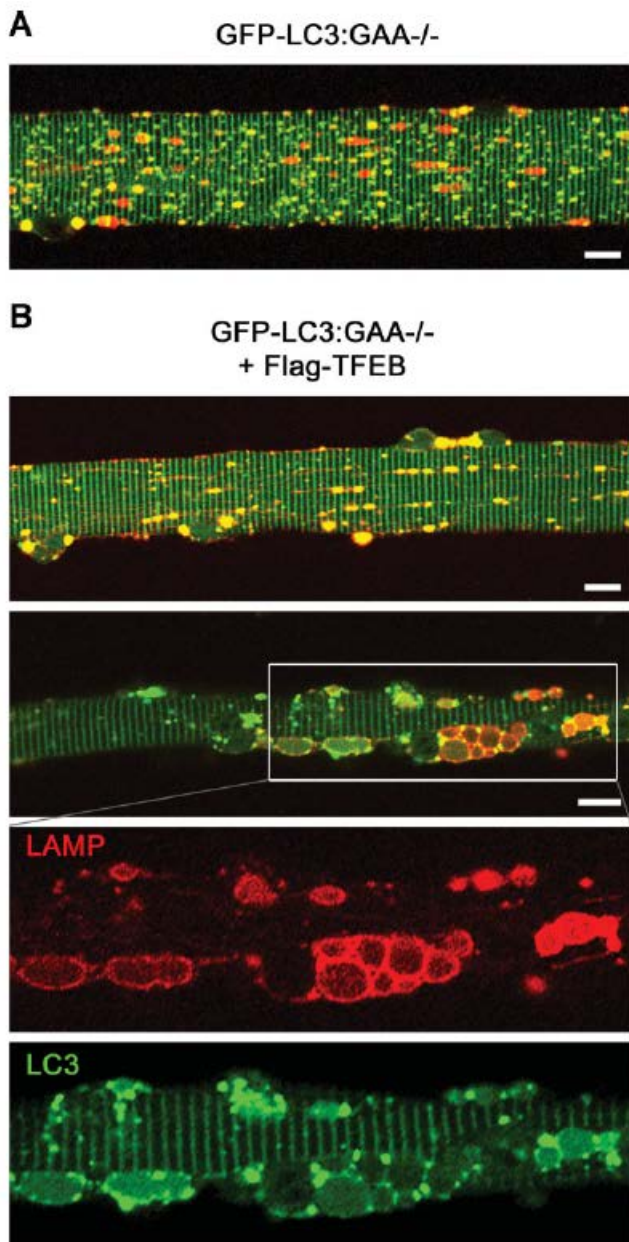


Fig. 34 TFEB stimulates lysosomal-autophagosomal fusion and clearance. Confocal microscopy images of live fibres from GFP-LC3:GAA^{-/-} mice. **(A)** Muscle was transfected with mCherry-LAMP1 only. The image (a single frame from the time-lapse series presented in Movie 5) shows lysosomes (red), LC3-positive autophagosomes (green) and a number of autolysosomes (yellow). **(B)** Muscle was transfected with Flag-TFEB and mCherry-LAMP1. Massive formation of autolysosomes is indicated by yellow structures; the three lower panels provide a snapshot of the process of exocytosis. The structures at the plasma membrane are labelled with both LC3 and LAMP1, indicating that they represent amphisomes (a product of fusion between autophagic vesicles and late endosomes) or autolysosomes (a product of fusion between autophagic vesicles and lysosomes). Bar: 10 μ m.

2.3 Suppression of autophagy attenuates TFEB-mediated cellular clearance in PD muscle

To address the role of autophagy in TFEB-mediated cellular clearance, GFP-TFEB and mCherry-LAMP1 were transfected into muscle-specific autophagy-deficient GAA ^{-/-} mice (Atg7:GAA DKO). All the signs of TFEB effects on lysosomal pathology were observed: size reduction, redistribution and docking along the plasma membrane (Fig. 35B), while no effects on lysosomal movement and fusion were observed when autophagy was suppressed. The maximum velocity of lysosomes was significantly lower than that in TFEB-treated PD mice (Fig. 36). Furthermore the TFEB-induced cellular clearance was lower in TFEB-treated autophagy deficient muscles than in controls, as indicated by a slight decrease in the number of large lysosomes (Fig. 36, bottom). This limited effect is particularly striking given the already decreased baseline lysosomal size (Fig. 35A and Fig.36) and a previously-reported reduction of glycogen levels in autophagy-deficient PD muscle [130]. Altogether these data suggest that autophagy is a prerequisite for efficient TFEB-mediated cellular clearance.

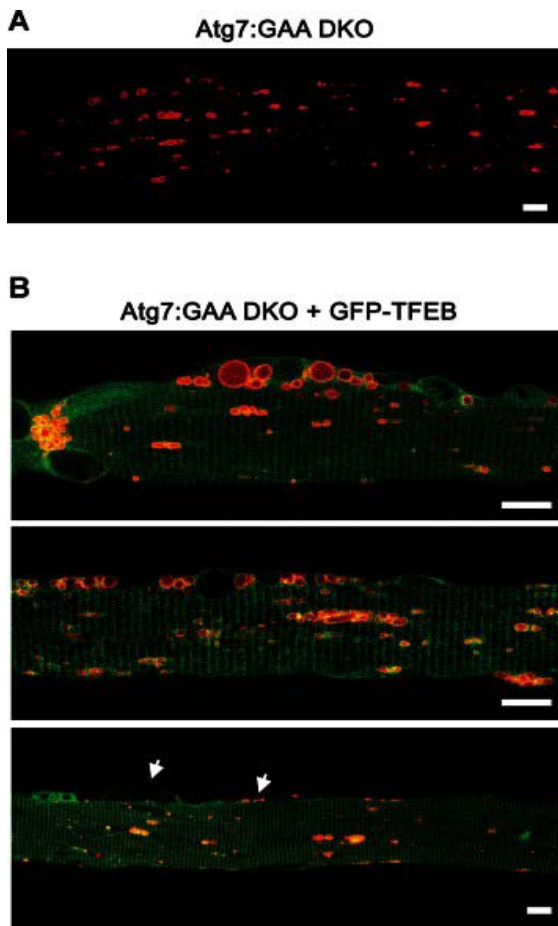


Fig. 35 TFEB promotes redistribution and docking of lysosomes to the plasma membrane in autophagy-deficient PD fibres. Confocal microscopy images of live fibres from muscle-specific autophagy-deficient GAA^{-/-} mice (Atg7:GAA DKO). (A) Muscle was transfected with mCherry-LAMP1 only. (B) Muscle was transfected with GFP-TFEB and mCherry-LAMP1 (Atg7:GAA DKO + GFP-TFEB). The TFEB-transfected fibres show realignment of the lysosomes and membrane detachment (most striking in top and bottom panels) similar to those in TFEB-transfected fibres from PD mice (see Fig 32 inset). Lysosomes can be seen in the space between the fibre and plasma membrane (arrows). Bar: 10 μ m.

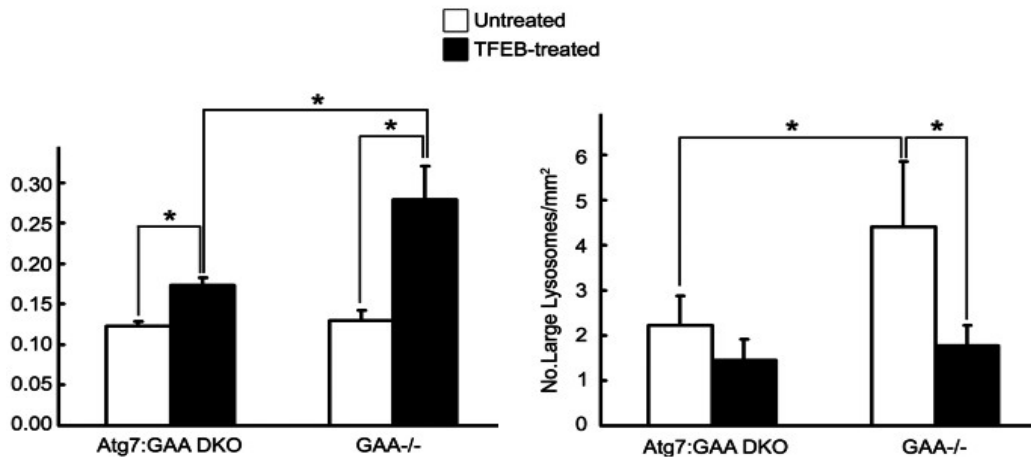


Fig. 36 TFEB increases lysosomal velocity in autophagy-deficient PD fibres. The mean maximum velocity of lysosomes (top) and the number of large (>3.5mm) lysosomes (bottom) in untreated and TFEB-treated autophagy-deficient Atg7:GAA DKO fibres. The increase in maximum velocity (41%) is significant ($p=2.729 \times 10^{-18}$; $n=57$ lysosomes for untreated; $n=52$ lysosomes for TFEB-treated), but there is only a slight trend toward smaller lysosomal size ($p=7.0 \times 10^{-2}$; $n=10$ fibres for untreated; $n=21$ fibres for TFEB-treated). The corresponding values from GAA-/- mice are presented for comparison (for TFEB-treated condition: $n=19$ lysosomes for velocity measurements, and $n=10$ fibres for the lysosomal size measurements). * indicates statistically significant differences ($p \leq 1.0 \times 10^{-5}$ for the top panel and $p \leq 0.01$ for the lower panel; Student's t-test).

2.4 Intramuscular injection of AAV 2.1-TFEB results in clearance of glycogen stores and amelioration of muscle pathology

We tested the effect of TFEB overexpression on muscle pathology *in vivo* by direct intramuscular injection of AAV 2.1-TFEB vectors in PD mice. Mice were injected at 1 month of age in three sites of the right gastrocnemius muscle, while the left gastrocnemius was injected with AAV 2.1-GFP vector and used as un-injected control. The animals were sacrificed 45 days after injection to allow maximal, sustained expression of the vector. Levels of TFEB, analysed by Real-Time PCR, were 10-fold higher in the AAV 2.1-TFEB injected muscles compared to those in controls.

TFEB expression resulted in near-complete clearance of accumulated glycogen (Fig. 37).

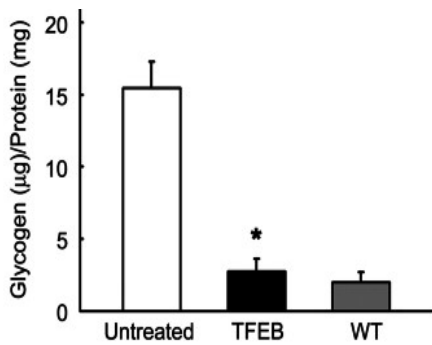


Fig. 37 Intramuscular injection of AAV2.1-TFEB in GAA ^{-/-} mice promotes glycogen clearance. Glycogen assay in TFEB-injected gastrocnemii and in the contralateral muscles. In TFEB-injected muscles glycogen levels were significantly decreased compared to those in untreated muscles. * indicates statistically significant differences ($p=1.0 \times 10^{-4}$; $n=6$; Student's t-test).

The reduction of glycogen stores in TFEB-treated muscles was also confirmed by PAS staining (Fig. 38) and by a decrease in the size of LAMP1 positive vesicles (Fig. 39).

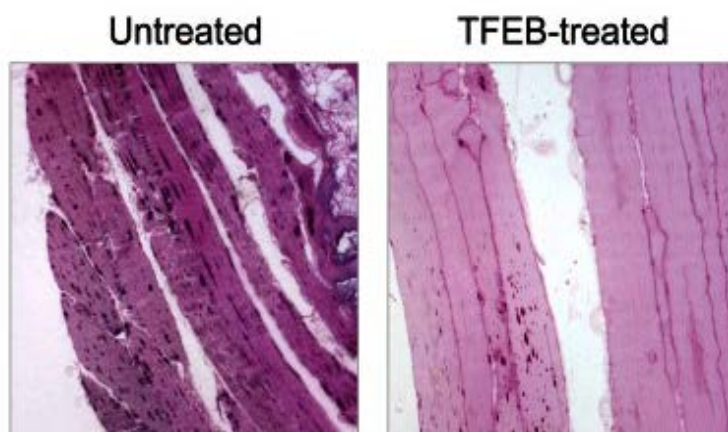


Fig. 38 Intramuscular injection of AAV2.1-TFEB in GAA ^{-/-} mice attenuates PD pathology. PAS staining of TFEB-treated muscle shows a reduction of lysosomal glycogen stores (puncta) compared to those in untreated muscle. Original magnification: 20x.

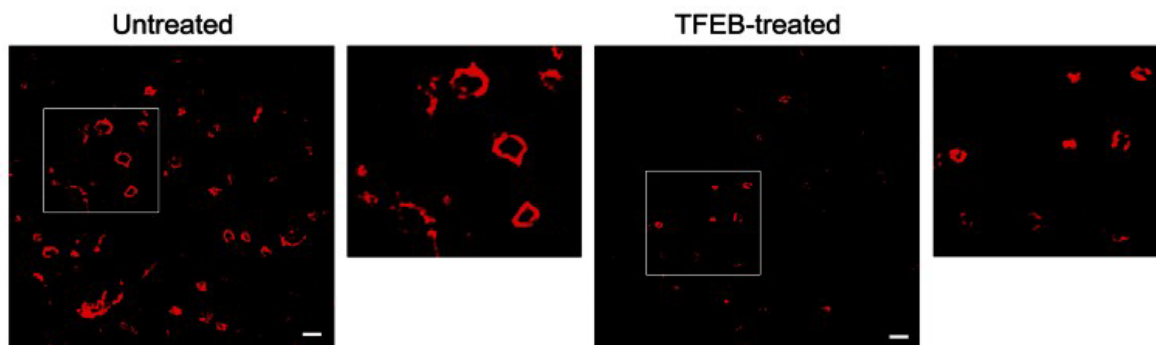


Fig. 39 Intramuscular injection of AAV2.1-TFEB in GAA ^{-/-} mice promotes clearance of enlarged lysosomes. LAMP1 staining of TFEB-injected gastrocnemii and of the contralateral untreated muscles. In TFEB-treated muscles, the size of LAMP1-positive vesicles was reduced. Bar: 2 μ m.

In addition we performed a more precise structural analysis of the autophagosomal/lysosomal compartment in TFEB treated muscle by EM analysis and found a significant improvement of muscle ultrastructure after TFEB overexpression. Specifically we observed a clear reduction in size and number of glycogen-containing lysosomes compared to those in PD muscle (Fig. 40A and B, left and middle panels). Furthermore, the intra-lysosomal electron-dense glycogen particles seen in untreated fibres (Fig. 40A, bottom left, asterisk) showed looser organization in TFEB-treated muscle (Fig. 40A, bottom right, asterisk).

In addition we observed an increased number of autophagosomes in close proximity to glycogen-containing organelles in TFEB-treated muscle (Fig. 40A bottom right, black arrows; Fig. 40B right panel). Moreover lysosomes frequently contained remnants of other intracellular organelles in their lumens (Fig. 40A bottom right, empty arrow), indicating active fusion with neighbouring autophagosomes.

The number of mitochondria in TFEB-treated fibres was comparable to that in untreated PD mice, and the size and morphology of mitochondria were normal (Fig.

40C).

These data on intramuscular injection indicate that TFEB is able to significantly rescue glycogen storage and morphological abnormalities.

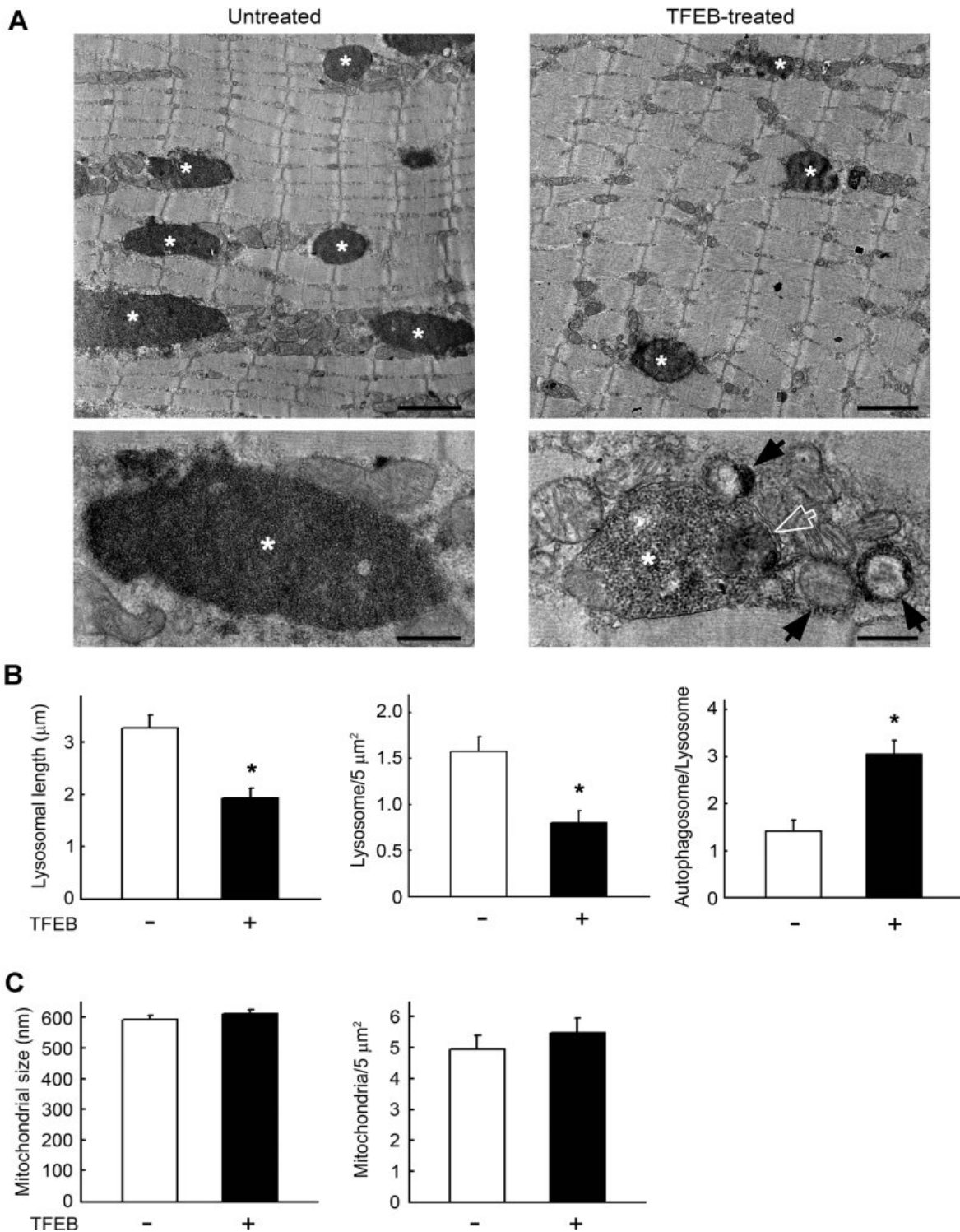


Fig. 40 Impact of TFEB on muscle fibre ultrastructure in GAA $-/-$ mice. (A) EM images of muscle injected with either AAV-GFP (untreated) or AAV-TFEB (TFEB-treated). Asterisks indicate glycogen-containing lysosomes. Bar: 1.5 μm (upper panels) and 0.45 μm (lower panels). Higher magnification images (lower panels) show that glycogen particles are less densely packed in TFEB-treated muscle. Black arrows indicate autophagosome profiles; the white empty arrow shows remnants of mitochondria engulfed by the lysosome. (B) Graphical presentations of lysosomal length (average \pm SE; $n=100$ lysosomes; $p=6.31 \times 10^{-5}$), the number of lysosomes per 5 mm^2 area of muscle fibre section (average \pm SE; $n=50$ fields; $p=4.80 \times 10^{-3}$), and the number of autophagosomes flanking glycogen-containing lysosomes (average \pm SE; $n=100$ lysosomes; $p=4.39 \times 10^{-5} < 0.001$). Student's t-test was used for each comparison. (C) Graphical presentations of mitochondrial size (average \pm SE; $n=100$) and the number of mitochondria per 5 mm^2 area of muscle fibre section (average \pm SE; $n=50$ fields). The differences were not significant by Student's t-test ($p=3.65 \times 10^{-1}$ and 4.27×10^{-1} , respectively).

DISCUSSION

In the first part of my PhD work I contributed to the identification of a specific pathway leading to cellular pathology in Lysosomal Storage Disorders, while in the second part of my PhD I used the knowledge derived from the previous work to develop a therapeutic approach for the treatment of LSDs.

In particular we demonstrated that in LSDs, secondary cholesterol accumulation causes a change in the endolysosomal membrane's organization and severely reduces the ability of lysosomes to efficiently fuse with other membranes. Specifically we showed that these cholesterol-dependent abnormalities cause defects in the fusion of lysosomes with endosomes and autophagosomes in two models of LSDs. We propose that this may represent a common early pathogenic mechanism underlying the endocytic jam observed in these disorders. Anyway there is still the need to clarify how the lysosomal primary defect leads to cholesterol accumulation, although some connections between these two pathogenic events have been identified in some LSDs [131, 132].

Our study also demonstrates that cholesterol accumulation in endolysosomal membranes impairs SNARE function. Physiological cholesterol-dependent clustering of SNAREs is implicated in defining the exocytotic sites on the plasma membrane in specialized secretory cells and in facilitating the exocytosis of synaptic vesicles [13, 113, 115, 116]. Moreover cholesterol has been shown to bind to synaptotagmin and promote synaptic vesicle biogenesis [112]. We argue that deleterious effects of

cholesterol accumulation in LSD membranes may result from the functional interaction of cholesterol with the SNARE apparatus.

In fact we demonstrate that endolysosomal cholesterol levels affect the membrane distribution of post-Golgi SNAREs involved in the fusion of lysosomes with endosomes and autophagosomes. Cholesterol accumulation in LSDs cells, and in cholesterol-loaded WT cells, induces SNAREs aggregation in cholesterol-enriched microdomains of endolysosomal membranes, resulting in the trapping of SNAREs in assembled complexes, and thus in a slower rate of SNARE recycling. Remarkably a previous study showed that the increase in cholesterol-enriched regions on plasma membranes inhibits SNARE function in exocytosis [133]. Cholesterol-dependent SNARE dysfunction may result from cholesterol's inhibition of SNARE dynamics in the endolysosomal membrane, a compartment normally deprived of cholesterol. This may in turn prevent SNAREs from correctly interacting with components of the fusion-recycling machinery. This hypothesis is supported by previous studies which demonstrated that cholesterol-mediated sub-compartmentalization of the lysosomal membrane protein LAMP-2A negatively affects chaperone-mediated autophagy [134].

In summary, in the first part of my PhD, I showed that cholesterol abnormalities in LSDs determine lysosomal fusion deficiency by affecting proper SNARE function.

We identified lysosomal dysfunction, due to cholesterol accumulation, as a possible pathogenic mechanism causing cellular damage and death in LSDs. From this discovery we aimed to positively modulate lysosomal compartment in order to obtain

cellular clearance in LSDs. We also took advantage of our lab's discovery of TFEB as a transcription factor that positively regulates lysosomal biogenesis and function [19]. We also showed that TFEB triggers lysosomal exocytosis and promotes cellular clearance in cellular models of LSDs [101]. From these discoveries we speculated the effectiveness of TFEB over-expression to increase lysosomal functions, prevalently lysosomal exocytosis, in order to obtain cellular clearance in an *in vivo* model of Pompe Disease.

We showed that TFEB efficiently triggers lysosomal exocytosis and promotes cellular clearance in muscle cells, isolated live muscle fibres and the whole muscle of PD mice.

The process of lysosomal exocytosis was initially ascribed to a subset of secretory lysosome, called lysosome-related organelles, which reside in particular cell types, such as haematopoietic cells or melanocytes [135]. Recently it has been shown that also conventional lysosomes can undergo fusion with plasma membrane and exocytosis [11] in a Ca^{2+} dependent process regulated by synaptotagmin. The process of conventional lysosome exocytosis is considered to be critical for the repair of plasma membrane lesions [136].

In addition lysosomal exocytosis has been implicated in mediating cellular clearance in cell models of several LSDs, such as metachromatic leukodystrophy and mucopolipidosis type I [137]. Furthermore it has been shown that lysosomal exocytosis is the mechanism by which 2-hydroxypropyl- β -cyclodextrin – an approved drug for yet another LSD, Niemann Pick type C (NPC) disease - alleviates cholesterol storage

in NPC cells [138].

Lysosomal exocytosis became an interesting therapeutic option for LSD after the discovery of TFEB [21, 101, 139]. Overexpression of TFEB induced lysosomal exocytosis in a mouse model of MSD and in cells derived from the murine models of MPS-III A, neuronal ceroid lipofuscinoses and MSD [101].

In the second part of my PhD I also helped demonstrate the positive effects of TFEB overexpression on cellular clearance in terminally differentiated multinucleated muscle cells and PD muscles. Specifically we showed that the hallmarks of PD (number of large glycogen-filled lysosomes and the amount of accumulated glycogen) were significantly reduced in both cultured myotubes and muscle fibres after TFEB overexpression, thus providing strong evidence of TFEB potential as a therapeutic target for PD.

In TFEB-treated myotubes the lysosomal marker LAMP1, that is typically present inside the cells, was seen on the outer plasma membrane. In addition we also showed a potential problem with high TFEB activity, as the expression of a constitutively active form of TFEB (TFEB S211A) invariably resulted in morphological changes of myotubes, perhaps because of massive expulsion of lysosomes.

Time-lapse confocal microscopy experiments on live fibre allowed us to track lysosomal movements and fusion in order to estimate the motility of lysosomes and to examine the interactions between lysosomes and autophagosomes after TFEB overexpression. Similarly to what we observed in the cellular system, we found that TFEB efficiently triggered lysosomal exocytosis and promoted cellular clearance.

The development of a new PD mouse model, the GFP-LC3:GAA $-/-$ strain, allowed us to address the effects of TFEB on autophagic accumulation. In fact defects in autophagy, a major lysosome-dependent degradative system, significantly contribute to the pathophysiology of several LSDs [95, 99, 100, 140]. In PD skeletal muscle, the autophagic defect is particularly striking, manifesting as a massive build-up that poses an additional problem for ERT.

Remarkably none of the TFEB-transfected fibres showed areas of autophagic build-up, which are so prominent in most non-transfected PD fibres. This condition suggests that TFEB may have rescued autophagic function in PD muscle. TFEB-treated fibres exhibited a significant increase in fusion between LC3 and LAMP1 positive vesicles, the appearance of multiple LC3/LAMP1-positive autophagolysosomes and docking of these double-positive structures to the plasma membrane. Altogether these data suggest that TFEB may rescue autophagy by stimulating the formation and secretion of autophagolysosomes, a product of lysosomal-autophagosomal fusion.

In fact we hypothesized that lysosomal exocytosis mediating cellular clearance in our model may be a process involving autophagy and secretion of autophagolysosomes. This hypothesis is supported by the attenuated effect of TFEB on lysosomal velocity and clearance observed in autophagy-deficient PD mice.

Moreover the absence of lysosomal-autophagosomal fusion and low expression of LAMP-1 in the build-up area suggest inefficient local lysosomal biogenesis. LAMPs are considered to be of key importance for lysosomal movement, maturation of

autophagosomes and lysosomal exocytosis [141]. Therefore, these low local LAMP1 concentrations in the build-up area may have far-reaching consequences. The build-up process appears to begin with the failure of a subset of lysosomes to fuse with autophagosomes, perhaps because of lysosomal rupture during muscle contractions. It is possible that this fusion defect and the paucity of the newly-formed lysosomes create conditions that favour expansion of the autophagic build-up. With the capacity to resolve both of these deficits by promoting lysosomal-autophagosomal fusion and biogenesis, TFEB is uniquely suited to remedy autophagic and lysosomal pathologies in PD.

MATERIALS AND METHODS

1 Lysosome isolation

Lysosomes were isolated from MEFs by magnetic chromatography using the two-step elution protocol described in [102]: Subconfluent 150 x 25-mm dishes were treated for 9h with FeDex medium at 37°C and subsequently maintained in normal Dulbecco's Modified Eagle medium (DMEM) for 16h. Cells were then collected by trypsin treatment, washed in buffer A (250 mM sucrose in 4 mM imidazole/HCl buffer pH 7.4) and then re-suspended in 750 µL of Buffer A+ (buffer A with the addition of 5 mM iodoacetamide and protease inhibitors). Plasma membranes were split by forcing cells twice through an 18G needle and five times through a 26G needle, and then the nuclei and broken membranes were pelleted by centrifugation at 600g for 5 min. The post-nuclear supernatant (PNS) was loaded on a MiniMACS column previously equilibrated with 10 mL of Buffer A and with the magnet attached. The unbound material was collected by gravity flow (flow-through) and the column washed with 10 mL of TBS (150 mM NaCl, 5 mM Tris-HCl pH 7.4). Lysosomes were broken by applying an hypotonic buffer B (5 mM Tris-HCl with the same protease inhibitor concentration as in buffer A+) and luminal proteins were eluted by gravity flow. Finally lysosomal membrane proteins were eluted by removing the magnet and adding a hypotonic buffer B+1% Triton X-114.

2 GP analysis and sucrose gradients

The GP analysis was performed following the protocol described in [108]: lysosomal membranes were stained for 15 min with 100 nM C-laurdan. Samples were excited at 385 nm, and emission spectra were recorded from 400 to 530 nm. Spectra of unstained samples were subtracted from the sample labelled with C-laurdan. The GP values were calculated according to following formula: $GP = \frac{I_{400-460} - I_{470-530}}{I_{400-460} + I_{470-530}}$, where $I_{400-460}$ and $I_{470-530}$ are the total fluorescence intensities recorded from 400 to 600 nm and from 470 to 530 nm, respectively.

For sucrose gradients, solubilised lysosomal membrane proteins were loaded at the bottom of a 9-mL discontinuous sucrose gradient (40, 35, 30, 25, 20, 15, 10 and 5%) in TNE (50 mM Tris-HCl pH 7.4, 150 mM NaCl and 5 mM EDTA) with the addition of 1% Triton X-114. Samples were ultracentrifuged at 39000 r.p.m. for 19 h at 4°C, and then 12 aliquots of 750 µL (corresponding to DRMs, intermediate and soluble fractions) were collected from the top to the bottom of the gradient and processed for cholesterol content, protein concentration and immunoblot analysis. Protein concentration was determined using the Dc Protein Assay kit (Bio-Rad). For immunoblot analysis, proteins from collected gradient fractions were precipitated in methanol/chloroform, resuspended in Laemmli buffer and subjected to SDS-PAGE to be probed with specific antibodies. Densitometry quantification of immunoblotted membranes was performed using the ImageJ program.

3 Phospholipid and cholesterol assay

Total lipids were purified by lysosomal membrane samples with a two-step Bligh and Dyer lipid extraction protocol. Dried lipids were suspended in methanol-chloroform (1:2) and then resolved on a TLC plate (Silica gel 60, MERCK). The developing solvent was methanol:chloroform:ammonia (65:35:5). Phospholipids and cholesterol were detected by Molybdenum blue staining (Sigma).

Phospholipids were quantified with a phosphate assay protocol: purified lipids were incubated 1h at 190°C with perchloric acid. After addition of ammonium molybdate (1%) and ascorbic acid (4%) the samples were incubated at 37°C for 2h. The amounts of phospholipids in each sample were calculated by reading absorbance at 800 nm.

Cholesterol content was determined using the Amplex Red Cholesterol Assay kit (Invitrogen) by following the manufacturer's protocol.

4 Antibodies

The following antibodies were used: rabbit polyclonal anti-LAMP1 (Sigma), rat monoclonal anti-Lamp1 (Santa Cruz Biotechnology), mouse monoclonal anti-Vti1b (BD Biosciences), rabbit polyclonal anti-Vti1b (Synaptic System), mouse monoclonal anti-SNARE TI VAMP1 1C7 (a kind gift from T. Galli, INSERM U950, Paris, France), mouse monoclonal anti-Flotillin (BD Biosciences), mouse monoclonal anti-

transferrin receptor (Zymed), rabbit polyclonal anti-GFP (Abcam), rabbit polyclonal anti-EpsinR (a kind gift from DJ Owen[121]), rabbit polyclonal anti-golgin 97 (a kind gift from AM De Matteis, TIGEM, Italy), rabbit polyclonal anti-SNAP23 (Synaptic System), rabbit polyclonal anti-Syntaxin 5 (Synaptic System), mouse monoclonal anti- α/β -SNAP (Synaptic System), anti-Sec22 (a kind gift from AM De Matteis, TIGEM, Italy), rabbit polyclonal anti-Rab7 (Abcam), rabbit polyclonal anti-EGFR (Santa Cruz Biotechnology) and rabbit polyclonal anti-cholera toxin B (Vibrant Lipid Rafts Labelling Kit, Molecular Probe), mouse anti-cytochrome (BD Bioscience), mouse anti-MyoD (BD Bioscience), mouse anti-Flag M2 (Sigma), mouse anti-myogenin (Dako), mouse anti-myosin heavy chain (Clontech), rabbit anti-Histone H3 (Cell Signalling) and rabbit anti-alpha tubulin (Abcam). Secondary horseradish peroxidase-conjugated antibodies (Pierce ECL), secondary antibodies for immunofluorescence were conjugated to Alexa Fluor dye 488 or 594 and 633 (Molecular Probes).

5 Transfections and drug treatments

MEFs were maintained in DMEM supplemented with 10% FBS and penicillin/streptomycin (normal culture medium). Sub-confluent MEFs were transfected using LipofectamineTM 2000 (Invitrogen) according to manufacturer's protocols. Drug treatments were performed as follows: M β CD (Sigma) at the final concentration of 10 mM in normal culture medium for 30 min at 37°C; water-soluble

cholesterol (M β CD-complexed cholesterol, Sigma) at the final concentration of 50 μ g/mL in normal culture medium for 90 min at 37°C; Bafilomycin A1 (Upstate) at final concentration of 200 nM in normal culture medium for 15h; and EGF (Sigma) at the final concentration of 100 ng/mL in normal culture medium for various time points (as indicated in Fig. 1).

6 Analysis of SNARE complexes

Purified lysosomal membrane samples in Triton X-114 were centrifuged at 15000 g (30 min at 4°C) to isolate the Triton-insoluble material (DRM fraction) and the Triton-soluble membrane proteins (soluble fraction). Both fractions together, with samples containing the total lysosomal membranes, were treated with Laemmli buffer and then divided in two aliquots. One aliquot was boiled (5 min at 100°C) to disrupt SDS complexes, whereas the other was kept at 4°C (non-boiled samples) before being subjected to SDS-PAGE.

Densitometry quantification of monomeric and complexed form of Vti1b was performed using the ImageJ program.

7 Immunoprecipitation

Cells were washed in PBS, and a post-nuclear supernatant was obtained by scraping cells in isotonic buffer and centrifuging them at 5000 g for 5 min. One volume of 2x

lysis buffer (50 mM Tris-HCl pH7.9, 200 mM NaCl, 1% Triton X-114, 1 mM EDTA, 50 mM HEPES and protease inhibitors from Sigma) was added to one volume of the supernatant, and the samples were then incubated with protein A Sepharose (Sigma) overnight, followed by 3h incubation with anti Vti1b antibodies (rabbit polyclonal). The immunoprecipitate was separated by centrifugation, boiled in Laemmli buffer and loaded onto 5-10% SDS-PAGE.

8 Plasmids

For the GFP-Vti1b plasmid construction, the corresponding amplified cDNA was cloned in the pEGFP-C3 vector (Clontech). The GFP-VAMP7 was a kind gift of M. D'Esposito (IGB, Naples, Italy). The GFP-GPI was a kind gift from J. Lippincott-Schwartz (NICHD, NIH, Bethesda, MD, USA). The tandem-fluorescent-LC3 (mRFP-GFP-LC3) plasmid was a kind gift from T. Yoshimori [1].

The plasmid containing the full-length 3xFlag-tagged human TFEB (referred to as Flag-TFEB) was described previously [19]. The plasmid containing the full-length rat Lamp1 (mCherry-Lamp1) was a kind gift of K. Zaal (Light Imaging Section, Office of Science and Technology, NIAMS, NIH, Bethesda, MD, USA). The plasmid containing GFP-TFEB was described previously [128].

9 Immunofluorescence analysis

Cells were washed three times in cold PBS and then fixed in 4% paraformaldehyde (PFA) for 15 min. Fixed cells were washed four times in cold PBS, permeabilized with 0.1% Saponin in blocking solution (0.5% BSA, 50 mM NH₄Cl and 0.02 NaN₃ in PBS) for 30 min and immunolabelled with appropriate primary and secondary antibodies. Cells were then washed four times in cold PBS and mounted in Vectashield mounting medium.

For dextran-Lamp1 co-immunofluorescence, cells were loaded with 100 µg/mL dextran (10000 MW) conjugated with the Alexa Fluor 594 dye (Molecular Probes) for 2h, then the dextran was removed and after additional 3h MEFs were fixed in 4% PFA and subjected to immunostaining with LAMP1.

Lipid raft immunofluorescence was performed using the Vibrant Lipid Rafts Labelling Kit (Molecular Probes) according to manufacturer's protocols.

Confocal microscopy was performed with a Zeiss LSM 510 microscope equipped with a Zeiss confocal-scanning laser using an x63 1.4 numerical aperture objective. The percentage of co-localizing fluorescence (merge) was quantified by using the “*co-localization*” module of the LSM 3.2 software (Zeiss).

For immunofluorescence on myotubes, cells were fixed in 2% paraformaldehyde (Electron Microscopy Sciences) for 15 min at room temperature, washed twice in PBS and permeabilized in 0.2% Triton X-100 (Sigma-Aldrich). Immunostaining with LAMP1, LC3 and Flag antibodies was done using M.O.M kit (Vector Laboratories) as described in [38]. The cell nuclei were stained with 2µg/mL Hoechst 33342 (Life Technologies) in PBS for 10 min. After staining, the cells were imaged on a Carl

Zeiss LSM 510 confocal microscope with a 40x or 63x oil immersion objective.

10 Immuno-electron microscopy

For EM on cells: MEFs transfected with GFP-VAMP7, GFP-GPI or treated with cholera toxin B (according to manufacturer's protocols of Vibrant Lipid Rafts Labelling Kit, Molecular Probe) to target GM1 ganglioside (a raft lipid), were washed with PBS and fixed in a solution of 4% PFA and 0.1% glutaraldehyde in 0.2M HEPES buffer (pH 7.4) for 15 min at room temperature, and then for additional 30 min in 4% PFA alone. After washing with PBS, cells were incubated for 30 min in blocking solution (50 mM NH₄Cl, 0.1% Saponin and 1% BSA in PBS) and overnight at 4°C with either anti-GFP or anti-cholera toxin B antibody diluted 1:100 in blocking solution. Cells were washed and incubated for 1h at room temperature with Nanogold-conjugated anti-rabbit IgG Fab fragment diluted 1:100 in blocking solution and processed according to the Nanogold enhancement protocol (Nanoprobes, Yaphank, NY, USA). Stained cells were embedded in Epon-812 and cut. The EM images were acquired from thin sections using an FEI Tecnai-12 electron microscope equipped with an ULTRA VIEW CCD digital camera (FEI, Eindhoven, The Netherlands).

For EM on muscles: muscle tissue was fixed in 1% glutaraldehyde in 0.2 M HEPES buffer and post-fixed in uranyl acetate and OsO₄. After dehydration through a graded series of ethanol and propilenoxide, the tissue was embedded in the Epoxy resin

(Epon 812, Sigma-Aldrich) and polymerized at 60°C for 72h. EM images of thin sections were acquired using a FEI Tecnai-12 electron microscope (FEI, Eindhoven, The Netherlands) equipped with a VELETTA CCD digital camera (Soft Imaging Systems GmbH, Munster, Germany). Quantification of the number of lysosome-like organelles and their dimensions, as well as the number of autophagosomes, was performed in 50 fields (of 5µm² dimensions) distributed randomly through the thin sections containing different fibres.

11 EGFR endocytosis

For EGFR endocytosis analysis, MEFs were starved in DMEM without the addition of FBS for 19h. After starvation, cells were treated with EGF to stimulate EGFR endocytosis. Cells were then collected at various time points (as indicated in Fig. 1) and lysed in RIPA buffer (50 mM Tris-HCl pH 7.5, 1% Triton X-100, 150 mM NaCl, 1 mM EDTA and 0.1% Na deoxycholate) with protease inhibitor (Sigma). Protein extracts were subjected to SDS-PAGE and immunoblotted using anti-EGFR antibody.

12 Analysis of autophagic flux

To monitor autophagic rate, MEFs were transfected with mRFP-GFP-LC3 that showed a GFP and RFP signal before the fusion with lysosomes. Only the the RFP

signal after fusion was exhibited due to the loss of GFP fluorescence within the acidic lysosomal environment. After 33h, cells were treated with bafilomycin for 15h to block lysosome-autophagosome fusion. After the removal of Bafilomycin from the culture medium the extent of lysosome-autophagosome fusion was evaluated after 1 and 3h by fixing in 4% PFA and measuring the green/red fluorescence ratio (GFP loss) in the regions corresponding to the vesicles, using a homemade MATLAB (The Mathworks) application (F. Formiggini).

13 FRAP analysis

For FRAP experiments, EGFP-Vti1b was transfected in MEFs cells grown on glass-bottomed microwell dishes (Mat-Tek). An area containing EGFP-Vti1b-positive endolysosomal clusters was photobleached with 100% of the argon laser power at 488 nm, resulting in a 70-80% reduction in the fluorescence intensity. The long-range motility of these groups of organelles was negligible. The recovery of fluorescence was monitored over time (300s) by scanning the bleached area at the conventional (low) laser power to minimize photobleaching during sampling. To analyse the rate of recovery, we compared the fluorescence of the photobleached area to that of an adjacent unbleached area of the same cell with similar fluorescence intensity. For each time point, the fluorescence of the bleached area was normalized to that of the corresponding control (unbleached) area to compensate for possible drift of the focal plane or photobleaching incurred during the low light sampling. For each

experimental FRAP curve, the $t_{1/2}$ value was calculated by fitting the data with the Boltzmann function. The FRAP experiments were performed at 37°C on Zeiss LSM 510 microscope equipped with a Zeiss confocal-scanning laser using a x63 1.4 numerical aperture objective

14 Isolation of single live myofibres

Isolation of single live myofibres from gastrocnemius and extensor digitorum longus (EDL) muscle from 3 to 4 month-old mice were isolated as described in [142]. Isolation of single live fibres from FDB muscle was done with the protocol described in [38]. Live fibres were either monitored by time-lapse microscopy or used for labelling acidic organelles (LysoTracker Red DND-99 100 nM, Life Technologies) or mitochondria (MitoTracker Red CMXRos 100 nM, Life Technologies). Alternatively fibres were fixed in 2% paraformaldehyde for 30 min and immunostained with anti-cytochrome c and anti-LAMP1 antibodies.

Live and fixed fibres were analysed on a LSM 510 confocal microscope (Carl Zeiss, Germany) equipped with Plan-Neofluar 40x oil immersion objective.

15 *In vivo* electroporation of skeletal muscle

Electric-pulse mediated transfer into FDB muscle was performed as described in [143]. Animals were sacrificed 4-6 days after the procedure. Live FDB fibres were isolated and analysed by time-lapse confocal microscopy.

16 Fibroblast and myoblast culture systems

Immortalized PD cell lines were derived from immortoGAA^{-/-} and immortoGFP-LC3:GAA^{-/-} mice. Single fibres from EDL muscle of 3-4 month-old mice were plated in each well (10 fibres per well) of a Matrigel-coated six-well plate in plating medium (10% horse serum in DMEM, 0.5% chick embryo extract, and 1x P/S/L-Glutamine) at 37°C, 5% CO₂. After 3 days, when the satellite cells began to migrate away from fibres, most of the medium (3/4) was replaced with proliferation medium (20% foetal bovine serum, 10% horse serum, 1% chick embryo extract, 1x P/S/L-glutamine in high glucose DMEM). Myogenic colonies were isolated with cloning cylinders (Corning) on day 5 or 6. Several individual myogenic clones were isolated and analysed for their proliferation capacity and the ability to differentiate into myotubes. To induce the expression of H-2K^b-tsA58 SV40 large T-antigen for immortalization of the satellite cells and myoblasts, recombinant IFN- γ (Life Technologies) was added to the proliferation medium (100 units/mL). The cells were then incubated at 33°C in an atmosphere of 5% CO₂. When myoblasts became nearly confluent, the medium was changed to differentiation medium (DMEM containing 2% horse serum, 0.5% chick embryo extract, 1x P/S/L-glutamine), and then the cells were moved to 37°C in an atmosphere of 5% CO₂. Myotubes began to form within 2 days. Glucose concentration was either 1 g/L (low) or 4.5 g/L (high). Myotubes survived in culture for 2-3 weeks. A wild type immortalized muscle cell line served

as the control.

17 Infection of myotubes with adenovirus expressing TFEB

Adenoviruses expressing either WT or mutant (S211A) TFEB were described previously [128]. Myotubes were infected with either adenovirus (Ad-null) or adenovirus expressing WT TFEB (Ad-TFEB) or S211A TFEB (Ad-TFEBmt) for 24, 48 or 72h.

18 Fluorescent glycogen detection, LDH measurements, *in situ* detection of apoptotic cells, surface LAMP1 analysis and acid phosphatase assay

Lysosomal glycogen in live cells was detected by the incorporation of 2-NBDG, a D-glucose fluorescent derivative (2-deoxyglucose), into glycogen as described in [144].

The amount of LDH released into the medium was assayed using the LDH-Cytotoxicity Assay Kit II (Abcam) according to the manufacturer's protocol.

Apoptotic cells were detected with TUNEL using the ApopTag® fluorescent Direct *In Situ* Apoptosis Detection Kit (Millipore).

Lysosomal exocytosis in TFEB-treated cell cultures was evaluated by the surface LAMP1 assay as previously described [101] and by the measurement of acid phosphatase released into the medium. The acid phosphatase assay was performed in cultures treated with Ad-TFEB for 2 days according to the standard procedure.

19 Western Blot on myotubes and muscle tissues

Myotubes or muscle tissues were homogenized in RIPA buffer (PBS containing 1% NP-40, 0.5% sodium deoxycholate, 0.1% SDS and protease/phosphatase inhibitor cocktail (Cell Signalling Technology)) and centrifuged for 30 min at 13000 rpm at 4°C. Alternatively, for nuclear/cytosolic fractionation, cells were lysed in 0.5% Triton X-100 buffer (50 mM Tris-HCl, 0.5% Triton X-100, 137.5 mM NaCl, 10% glycerol, 5 mM EDTA and protease and phosphatase inhibitors) and centrifuged at 3000 rpm at 4°C for 5 min. The supernatant constituted the cytosolic fraction. The pellet was then washed with 0.5% Triton X-100 buffer, re-suspended in Triton X-100 buffer with 0.5% SDS, sonicated, and centrifuged at 13000 rpm for 15 min at 4°C. The supernatant constituted the nuclear fraction. Protein concentrations were measured using the Bio-Rad Protein Assay (Bio-Rad Laboratories). Western blots were performed according to standard procedures.

20 Intramuscular injection of AAV-TFEB, muscle staining and glycogen assay

Six 1-month-old GAA ^{-/-} mice were injected with a total dose of 10¹¹ GC of AAV 2/1 TFEB vector preparation into three sites of the right gastrocnemius (three injections of 30 µL each) using a Hamilton syringe. Equivalent doses of AAV 2/1 CMV-EGFP or equal volumes of PBS were injected into the controlateral muscle. Animals were sacrificed 45 days after injection and perfused with PBS.

Gastrocnemii, free from neighbouring muscle and connective tissue, were isolated and analysed. Part of the sample was used to test the levels of TFEB expression by RT-PCR. For morphologic analysis, muscles were frozen in liquid nitrogen-cooled isopentane. Immunostaining of 10 µm sections was performed using anti-LAMP1 (1:500 Abcam) and anti-Caspase-3 Active (1:500 R&D Systems) antibodies.

Apoptotic cells were detected with TUNEL using the Fluorescein In Situ Cell Death Detection Kit (Roche) according to the supplier's protocol. Muscle sections were mounted with Vectashield, and photographs were taken using a fluorescence microscope Zeiss Axioplan 2 integrated with the AxioCam MR camera.

Haematoxylin-eosin and PAS staining were performed according to standard procedures.

Glycogen concentration was assayed in muscle lysates by measuring the amount of glucose released after digestion with amyloglucosidase (*Aspergillus niger*) using a commercial kit (BioVision).

Data were expressed as µg of glycogen/mg of protein.

BIBLIOGRAPHY

1. Kimura, S., T. Noda, and T. Yoshimori, *Dissection of the autophagosome maturation process by a novel reporter protein, tandem fluorescent-tagged LC3*. *Autophagy*, 2007. **3**(5): p. 452-60.
2. Duve, C.d., *Duve, C. de*, in *In Sub-cellular Particles*, T. Hayashi, Editor 1959, Ronald Press: New York. p. pp. 128-159.
3. Eskelinen, E.L., Y. Tanaka, and P. Saftig, *At the acidic edge: emerging functions for lysosomal membrane proteins*. *Trends Cell Biol*, 2003. **13**(3): p. 137-45.
4. Bleistein, J., H.G. Heidrich, and H. Debuch, *The phospholipids of liver lysosomes from untreated rats*. *Hoppe Seylers Z Physiol Chem*, 1980. **361**(4): p. 595-7.
5. Forster, S., et al., *Translocation of sugars across the lysosome membrane*. *Biochem Soc Trans*, 1989. **17**(3): p. 441.
6. Fukuda, M., *Lysosomal membrane glycoproteins. Structure, biosynthesis, and intracellular trafficking*. *J Biol Chem*, 1991. **266**(32): p. 21327-30.
7. Lewis, V., et al., *Glycoproteins of the lysosomal membrane*. *J Cell Biol*, 1985. **100**(6): p. 1839-47.
8. Barriocanal, J.G., et al., *Biosynthesis, glycosylation, movement through the Golgi system, and transport to lysosomes by an N-linked carbohydrate-independent mechanism of three lysosomal integral membrane proteins*. *J Biol Chem*, 1986. **261**(35): p. 16755-63.
9. Journet, A., et al., *Proteomic analysis of human lysosomes: application to monocytic and breast cancer cells*. *Proteomics*, 2002. **2**(8): p. 1026-40.
10. Bonifacino, J.S. and L.M. Traub, *Signals for sorting of transmembrane proteins to endosomes and lysosomes*. *Annu Rev Biochem*, 2003. **72**: p. 395-447.
11. Andrews, N.W., *Regulated secretion of conventional lysosomes*. *Trends Cell Biol*, 2000.

- 10**(8): p. 316-21.
12. Huynh, C. and N.W. Andrews, *The small chemical vacuolin-1 alters the morphology of lysosomes without inhibiting Ca²⁺-regulated exocytosis*. EMBO Rep, 2005. **6**(9): p. 843-7.
 13. Bossi, G. and G.M. Griffiths, *CTL secretory lysosomes: biogenesis and secretion of a harmful organelle*. Semin Immunol, 2005. **17**(1): p. 87-94.
 14. Jaiswal, J.K., N.W. Andrews, and S.M. Simon, *Membrane proximal lysosomes are the major vesicles responsible for calcium-dependent exocytosis in nonsecretory cells*. J Cell Biol, 2002. **159**(4): p. 625-35.
 15. Rodriguez, A., et al., *cAMP regulates Ca²⁺-dependent exocytosis of lysosomes and lysosome-mediated cell invasion by trypanosomes*. J Biol Chem, 1999. **274**(24): p. 16754-9.
 16. Rodriguez, A., et al., *Lysosomes behave as Ca²⁺-regulated exocytic vesicles in fibroblasts and epithelial cells*. J Cell Biol, 1997. **137**(1): p. 93-104.
 17. Dell'Angelica, E.C., et al., *Lysosome-related organelles*. FASEB J, 2000. **14**(10): p. 1265-78.
 18. Storrie, B. and M. Desjardins, *The biogenesis of lysosomes: is it a kiss and run, continuous fusion and fission process?* Bioessays, 1996. **18**(11): p. 895-903.
 19. Sardiello, M., et al., *A gene network regulating lysosomal biogenesis and function*. Science, 2009. **325**(5939): p. 473-7.
 20. Palmieri, M., et al., *Characterization of the CLEAR network reveals an integrated control of cellular clearance pathways*. Hum Mol Genet, 2011. **20**(19): p. 3852-66.
 21. Settembre, C. and A. Ballabio, *TFEB regulates autophagy: an integrated coordination of cellular degradation and recycling processes*. Autophagy, 2011. **7**(11): p. 1379-81.
 22. Settembre, C., et al., *A lysosome-to-nucleus signalling mechanism senses and regulates the lysosome via mTOR and TFEB*. EMBO J, 2012. **31**(5): p. 1095-108.
 23. Austin, J.H., *Metachromatic and globoid body leukodystrophies*. Clin Proc Child Hosp Dist Columbia, 1966. **22**(8): p. 223-7.

24. Baenziger, J.U., *A major step on the road to understanding a unique posttranslational modification and its role in a genetic disease*. Cell, 2003. **113**(4): p. 421-2.
25. Parenti, G., G. Meroni, and A. Ballabio, *The sulfatase gene family*. Curr Opin Genet Dev, 1997. **7**(3): p. 386-91.
26. Meroni, G., et al., *Characterization of a cluster of sulfatase genes on Xp22.3 suggests gene duplications in an ancestral pseudoautosomal region*. Hum Mol Genet, 1996. **5**(4): p. 423-31.
27. Fraldi, A., et al., *Multistep, sequential control of the trafficking and function of the multiple sulfatase deficiency gene product, SUMF1 by PDI, ERGIC-53 and ERp44*. Hum Mol Genet, 2008. **17**(17): p. 2610-21.
28. Zito, E., et al., *Sulfatase modifying factor 1 trafficking through the cells: from endoplasmic reticulum to the endoplasmic reticulum*. EMBO J, 2007. **26**(10): p. 2443-53.
29. Settembre, C., et al., *Systemic inflammation and neurodegeneration in a mouse model of multiple sulfatase deficiency*. Proc Natl Acad Sci U S A, 2007. **104**(11): p. 4506-11.
30. Blanco-Aguirre, M.E., et al., *Unusual clinical presentation in two cases of multiple sulfatase deficiency*. Pediatr Dermatol, 2001. **18**(5): p. 388-92.
31. Kakkis, E.D., et al., *Enzyme-replacement therapy in mucopolysaccharidosis I*. N Engl J Med, 2001. **344**(3): p. 182-8.
32. Meikle, P.J., et al., *Prevalence of lysosomal storage disorders*. JAMA, 1999. **281**(3): p. 249-54.
33. Bhattacharyya, R., et al., *A novel missense mutation in lysosomal sulfamidase is the basis of MPS III A in a spontaneous mouse mutant*. Glycobiology, 2001. **11**(1): p. 99-103.
34. Crawley, A.C., et al., *Characterization of a C57BL/6 congenic mouse strain of mucopolysaccharidosis type IIIA*. Brain Res, 2006. **1104**(1): p. 1-17.
35. King, B., et al., *Validation of a heparan sulfate-derived disaccharide as a marker of accumulation in murine mucopolysaccharidosis type IIIA*. Mol Genet Metab, 2006. **87**(2): p.

107-12.

36. Kroos, M., et al., *The genotype-phenotype correlation in Pompe disease*. Am J Med Genet C Semin Med Genet, 2012. **160C**(1): p. 59-68.
37. van der Ploeg, A.T. and A.J. Reuser, *Pompe's disease*. Lancet, 2008. **372**(9646): p. 1342-53.
38. Raben, N., et al., *Deconstructing Pompe disease by analyzing single muscle fibres: to see a world in a grain of sand*. Autophagy, 2007. **3**(6): p. 546-52.
39. Raben, N., A. Roberts, and P.H. Plotz, *Role of autophagy in the pathogenesis of Pompe disease*. Acta Myol, 2007. **26**(1): p. 45-8.
40. Raben, N., et al., *Autophagy and mitochondria in Pompe disease: nothing is so new as what has long been forgotten*. Am J Med Genet C Semin Med Genet, 2012. **160C**(1): p. 13-21.
41. Raben, N., et al., *Targeted disruption of the acid alpha-glucosidase gene in mice causes an illness with critical features of both infantile and adult human glycogen storage disease type II*. J Biol Chem, 1998. **273**(30): p. 19086-92.
42. Fratantoni, J.C., C.W. Hall, and E.F. Neufeld, *Hurler and Hunter syndromes: mutual correction of the defect in cultured fibroblasts*. Science, 1968. **162**(3853): p. 570-2.
43. Yu, W.H., et al., *Short-term enzyme replacement in the murine model of Sanfilippo syndrome type B*. Mol Genet Metab, 2000. **71**(4): p. 573-80.
44. Crawley, A.C., et al., *Enzyme replacement therapy in a feline model of Maroteaux-Lamy syndrome*. J Clin Invest, 1996. **97**(8): p. 1864-73.
45. Byers, S., et al., *Enzyme replacement therapy in a feline model of MPS VI: modification of enzyme structure and dose frequency*. Pediatr Res, 2000. **47**(6): p. 743-9.
46. Vogler, C., et al., *Enzyme replacement in murine mucopolysaccharidosis type VII: neuronal and glial response to beta-glucuronidase requires early initiation of enzyme replacement therapy*. Pediatr Res, 1999. **45**(6): p. 838-44.
47. Ioannou, Y.A., et al., *Fabry disease: preclinical studies demonstrate the effectiveness of alpha-galactosidase A replacement in enzyme-deficient mice*. Am J Hum Genet, 2001.

- 68(1): p. 14-25.
48. Miranda, S.R., et al., *Infusion of recombinant human acid sphingomyelinase into niemann-pick disease mice leads to visceral, but not neurological, correction of the pathophysiology.* FASEB J, 2000. **14**(13): p. 1988-95.
 49. Bijvoet, A.G., et al., *Human acid alpha-glucosidase from rabbit milk has therapeutic effect in mice with glycogen storage disease type II.* Hum Mol Genet, 1999. **8**(12): p. 2145-53.
 50. O'Connor, L.H., et al., *Enzyme replacement therapy for murine mucopolysaccharidosis type VII leads to improvements in behavior and auditory function.* J Clin Invest, 1998. **101**(7): p. 1394-400.
 51. Scherrmann, J.M., *Drug delivery to brain via the blood-brain barrier.* Vascul Pharmacol, 2002. **38**(6): p. 349-54.
 52. Alisky, J.M., C.I. van de Wetering, and B.L. Davidson, *Widespread dispersal of cholera toxin subunit b to brain and spinal cord neurons following systemic delivery.* Exp Neurol, 2002. **178**(1): p. 139-46.
 53. Jakobsson, J., et al., *Targeted transgene expression in rat brain using lentiviral vectors.* J Neurosci Res, 2003. **73**(6): p. 876-85.
 54. Sorrentino, N.C., et al., *A highly secreted sulphamidase engineered to cross the blood-brain barrier corrects brain lesions of mice with mucopolysaccharidoses type IIIA.* EMBO Mol Med, 2013. **5**(5): p. 675-90.
 55. Dahms, N.M., P. Lobel, and S. Kornfeld, *Mannose 6-phosphate receptors and lysosomal enzyme targeting.* J Biol Chem, 1989. **264**(21): p. 12115-8.
 56. Walkley, S.U., et al., *Bone marrow transplantation corrects the enzyme defect in neurons of the central nervous system in a lysosomal storage disease.* Proc Natl Acad Sci U S A, 1994. **91**(8): p. 2970-4.
 57. Kennedy, D.W. and J.L. Abkowitz, *Kinetics of central nervous system microglial and macrophage engraftment: analysis using a transgenic bone marrow transplantation model.*

- Blood, 1997. **90**(3): p. 986-93.
58. Krall, W.J., et al., *Cells expressing human glucocerebrosidase from a retroviral vector repopulate macrophages and central nervous system microglia after murine bone marrow transplantation*. Blood, 1994. **83**(9): p. 2737-48.
59. Lawson, L.J., V.H. Perry, and S. Gordon, *Turnover of resident microglia in the normal adult mouse brain*. Neuroscience, 1992. **48**(2): p. 405-15.
60. Walkley, S.U. and K. Dobrenis, *Bone marrow transplantation for lysosomal diseases*. Lancet, 1995. **345**(8962): p. 1382-3.
61. Braun, S.E., et al., *Metabolic correction and cross-correction of mucopolysaccharidosis type II (Hunter syndrome) by retroviral-mediated gene transfer and expression of human iduronate-2-sulfatase*. Proc Natl Acad Sci U S A, 1993. **90**(24): p. 11830-4.
62. Vellodi, A., et al., *Bone marrow transplantation for mucopolysaccharidosis type I: experience of two British centres*. Arch Dis Child, 1997. **76**(2): p. 92-9.
63. Hoogerbrugge, P.M. and J.M. Vossen, *BMT for isolated central nervous system relapse in children with ALL*. Bone Marrow Transplant, 1995. **16**(6): p. 859-60.
64. Hoogerbrugge, P.M. and D. Valerio, *Bone marrow transplantation and gene therapy for lysosomal storage diseases*. Bone Marrow Transplant, 1998. **21 Suppl 2**: p. S34-6.
65. D'Azzo, A., *Gene transfer strategies for correction of lysosomal storage disorders*. Acta Haematol, 2003. **110**(2-3): p. 71-85.
66. Ou, R.M., et al., *[Allogeneic hematopoietic stem cell transplantation for the treatment of mucopolysaccharidosis type I: a case report]*. Zhongguo Dang Dai Er Ke Za Zhi, 2006. **8**(3): p. 181-3.
67. Ferrara, M.L., et al., *Canine fucosidosis: a model for retroviral gene transfer into haematopoietic stem cells*. Neuromuscul Disord, 1997. **7**(5): p. 361-6.
68. Lutzko, C., et al., *Gene therapy for canine alpha-L-iduronidase deficiency: in utero adoptive transfer of genetically corrected hematopoietic progenitors results in engraftment*

- but not amelioration of disease.* Hum Gene Ther, 1999. **10**(9): p. 1521-32.
69. Dunbar, C.E., et al., *Retroviral transfer of the glucocerebrosidase gene into CD34+ cells from patients with Gaucher disease: in vivo detection of transduced cells without myeloablation.* Hum Gene Ther, 1998. **9**(17): p. 2629-40.
70. Ohashi, K., et al., *Modified infusion procedures affect recombinant adeno-associated virus vector type 2 transduction in the liver.* Hum Gene Ther, 2005. **16**(3): p. 299-306.
71. Lieber, A., et al., *Integrating adenovirus-adeno-associated virus hybrid vectors devoid of all viral genes.* J Virol, 1999. **73**(11): p. 9314-24.
72. Kanaji, A., et al., *Improvement of skeletal lesions in mice with mucopolysaccharidosis type VII by neonatal adenoviral gene transfer.* Mol Ther, 2003. **8**(5): p. 718-25.
73. Kamata, Y., et al., *Long-term normalization in the central nervous system, ocular manifestations, and skeletal deformities by a single systemic adenovirus injection into neonatal mice with mucopolysaccharidosis VII.* Gene Ther, 2003. **10**(5): p. 406-14.
74. Ghodsi, A., et al., *Extensive beta-glucuronidase activity in murine central nervous system after adenovirus-mediated gene transfer to brain.* Hum Gene Ther, 1998. **9**(16): p. 2331-40.
75. Fraldi, A., et al., *Functional correction of CNS lesions in an MPS-IIIa mouse model by intracerebral AAV-mediated delivery of sulfamidase and SUMF1 genes.* Hum Mol Genet, 2007. **16**(22): p. 2693-702.
76. Ponder, K.P., et al., *Therapeutic neonatal hepatic gene therapy in mucopolysaccharidosis VII dogs.* Proc Natl Acad Sci U S A, 2002. **99**(20): p. 13102-7.
77. Xu, L., et al., *Evaluation of pathological manifestations of disease in mucopolysaccharidosis VII mice after neonatal hepatic gene therapy.* Mol Ther, 2002. **6**(6): p. 745-58.
78. Krentler, C., et al., *Lysosomal membrane proteins do not bind to mannose-6-phosphate-specific receptors.* Biol Chem Hoppe Seyler, 1986. **367**(2): p. 141-5.
79. Fan, J.Q. and S. Ishii, *Cell-based screening of active-site specific chaperone for the*

- treatment of Fabry disease. Methods Enzymol*, 2003. **363**: p. 412-20.
80. Lev, M. and K.S. Sundaram, *Gaucher's disease*. *N Engl J Med*, 1987. **317**(9): p. 572.
81. Biswas, S. and S.M. LeVine, *Substrate-reduction therapy enhances the benefits of bone marrow transplantation in young mice with globoid cell leukodystrophy*. *Pediatr Res*, 2002. **51**(1): p. 40-7.
82. Jeyakumar, M., et al., *Enhanced survival in Sandhoff disease mice receiving a combination of substrate deprivation therapy and bone marrow transplantation*. *Blood*, 2001. **97**(1): p. 327-9.
83. Futerman, A.H. and G. van Meer, *The cell biology of lysosomal storage disorders*. *Nat Rev Mol Cell Biol*, 2004. **5**(7): p. 554-65.
84. Yang, A.J., et al., *Loss of endosomal/lysosomal membrane impermeability is an early event in amyloid Abeta1-42 pathogenesis*. *J Neurosci Res*, 1998. **52**(6): p. 691-8.
85. Castino, R., M. Demoz, and C. Isidoro, *Destination 'lysosome': a target organelle for tumour cell killing?* *J Mol Recognit*, 2003. **16**(5): p. 337-48.
86. Hannun, Y.A. and R.M. Bell, *Functions of sphingolipids and sphingolipid breakdown products in cellular regulation*. *Science*, 1989. **243**(4890): p. 500-7.
87. Wada, R., C.J. Tiffit, and R.L. Proia, *Microglial activation precedes acute neurodegeneration in Sandhoff disease and is suppressed by bone marrow transplantation*. *Proc Natl Acad Sci U S A*, 2000. **97**(20): p. 10954-9.
88. Myerowitz, R., et al., *Molecular pathophysiology in Tay-Sachs and Sandhoff diseases as revealed by gene expression profiling*. *Hum Mol Genet*, 2002. **11**(11): p. 1343-50.
89. Jeyakumar, M., et al., *Central nervous system inflammation is a hallmark of pathogenesis in mouse models of GM1 and GM2 gangliosidosis*. *Brain*, 2003. **126**(Pt 4): p. 974-87.
90. Levine, B. and D.J. Klionsky, *Development by self-digestion: molecular mechanisms and biological functions of autophagy*. *Dev Cell*, 2004. **6**(4): p. 463-77.
91. Mizushima, N., *Autophagy: process and function*. *Genes Dev*, 2007. **21**(22): p. 2861-73.

92. Mizushima, N. and D.J. Klionsky, *Protein turnover via autophagy: implications for metabolism*. *Annu Rev Nutr*, 2007. **27**: p. 19-40.
93. Hara, T., et al., *Suppression of basal autophagy in neural cells causes neurodegenerative disease in mice*. *Nature*, 2006. **441**(7095): p. 885-9.
94. Komatsu, M., et al., *Loss of autophagy in the central nervous system causes neurodegeneration in mice*. *Nature*, 2006. **441**(7095): p. 880-4.
95. Settembre, C., et al., *A block of autophagy in lysosomal storage disorders*. *Hum Mol Genet*, 2008. **17**(1): p. 119-29.
96. Tanaka, Y., et al., *Accumulation of autophagic vacuoles and cardiomyopathy in LAMP-2-deficient mice*. *Nature*, 2000. **406**(6798): p. 902-6.
97. Lu, Z., et al., *Participation of autophagy in the degeneration process of rat hepatocytes after transplantation following prolonged cold preservation*. *Arch Histol Cytol*, 2005. **68**(1): p. 71-80.
98. Koike, M., et al., *Participation of autophagy in storage of lysosomes in neurons from mouse models of neuronal ceroid-lipofuscinoses (Batten disease)*. *Am J Pathol*, 2005. **167**(6): p. 1713-28.
99. Cao, Y., et al., *Autophagy is disrupted in a knock-in mouse model of juvenile neuronal ceroid lipofuscinosis*. *J Biol Chem*, 2006. **281**(29): p. 20483-93.
100. Fukuda, T., et al., *Dysfunction of endocytic and autophagic pathways in a lysosomal storage disease*. *Ann Neurol*, 2006. **59**(4): p. 700-8.
101. Medina, D.L., et al., *Transcriptional activation of lysosomal exocytosis promotes cellular clearance*. *Dev Cell*, 2011. **21**(3): p. 421-30.
102. Diettrich, O., et al., *Application of magnetic chromatography to the isolation of lysosomes from fibroblasts of patients with lysosomal storage disorders*. *FEBS Lett*, 1998. **441**(3): p. 369-72.
103. Simons, K. and E. Ikonen, *Functional rafts in cell membranes*. *Nature*, 1997. **387**(6633): p.

569-72.

104. Simons, K. and W.L. Vaz, *Model systems, lipid rafts, and cell membranes*. Annu Rev Biophys Biomol Struct, 2004. **33**: p. 269-95.
105. Rajendran, L. and K. Simons, *Lipid rafts and membrane dynamics*. J Cell Sci, 2005. **118**(Pt 6): p. 1099-102.
106. Lingwood, D. and K. Simons, *Lipid rafts as a membrane-organizing principle*. Science, 2010. **327**(5961): p. 46-50.
107. Lingwood, D. and K. Simons, *Detergent resistance as a tool in membrane research*. Nat Protoc, 2007. **2**(9): p. 2159-65.
108. Kaiser, H.J., et al., *Order of lipid phases in model and plasma membranes*. Proc Natl Acad Sci U S A, 2009. **106**(39): p. 16645-50.
109. Suzuki, K., *Lysosomal Disease*, L.P. Graham DI, Editor 2002. p. 653–735.
110. Weber, T., et al., *SNAREpins: minimal machinery for membrane fusion*. Cell, 1998. **92**(6): p. 759-72.
111. Jahn, R. and R.H. Scheller, *SNAREs--engines for membrane fusion*. Nat Rev Mol Cell Biol, 2006. **7**(9): p. 631-43.
112. Thiele, C., et al., *Cholesterol binds to synaptophysin and is required for biogenesis of synaptic vesicles*. Nat Cell Biol, 2000. **2**(1): p. 42-9.
113. Chamberlain, L.H., R.D. Burgoyne, and G.W. Gould, *SNARE proteins are highly enriched in lipid rafts in PC12 cells: implications for the spatial control of exocytosis*. Proc Natl Acad Sci U S A, 2001. **98**(10): p. 5619-24.
114. Lang, T., *SNARE proteins and 'membrane rafts'*. J Physiol, 2007. **585**(Pt 3): p. 693-8.
115. Puri, N. and P.A. Roche, *Ternary SNARE complexes are enriched in lipid rafts during mast cell exocytosis*. Traffic, 2006. **7**(11): p. 1482-94.
116. Lang, T., et al., *SNAREs are concentrated in cholesterol-dependent clusters that define docking and fusion sites for exocytosis*. EMBO J, 2001. **20**(9): p. 2202-13.

117. Pryor, P.R., et al., *Combinatorial SNARE complexes with VAMP7 or VAMP8 define different late endocytic fusion events*. EMBO Rep, 2004. **5**(6): p. 590-5.
118. Zhang, M., et al., *Rab7: roles in membrane trafficking and disease*. Biosci Rep, 2009. **29**(3): p. 193-209.
119. Hirst, J., et al., *EpsinR is an adaptor for the SNARE protein Vti1b*. Mol Biol Cell, 2004. **15**(12): p. 5593-602.
120. Tran, T.H., Q. Zeng, and W. Hong, *VAMP4 cycles from the cell surface to the trans-Golgi network via sorting and recycling endosomes*. J Cell Sci, 2007. **120**(Pt 6): p. 1028-41.
121. Miller, S.E., et al., *A SNARE-adaptor interaction is a new mode of cargo recognition in clathrin-coated vesicles*. Nature, 2007. **450**(7169): p. 570-4.
122. Pryor, P.R., et al., *Molecular basis for the sorting of the SNARE VAMP7 into endocytic clathrin-coated vesicles by the ArfGAP Hrb*. Cell, 2008. **134**(5): p. 817-27.
123. Sollner, T., et al., *SNAP receptors implicated in vesicle targeting and fusion*. Nature, 1993. **362**(6418): p. 318-24.
124. Littleton, J.T., et al., *SNARE-complex disassembly by NSF follows synaptic-vesicle fusion*. Proc Natl Acad Sci U S A, 2001. **98**(21): p. 12233-8.
125. Hanson, P.I., et al., *The N-ethylmaleimide-sensitive fusion protein and alpha-SNAP induce a conformational change in syntaxin*. J Biol Chem, 1995. **270**(28): p. 16955-61.
126. McMahon, H.T. and T.C. Sudhof, *Synaptic core complex of synaptobrevin, syntaxin, and SNAP25 forms high affinity alpha-SNAP binding site*. J Biol Chem, 1995. **270**(5): p. 2213-7.
127. Barszczewski, M., et al., *A novel site of action for alpha-SNAP in the SNARE conformational cycle controlling membrane fusion*. Mol Biol Cell, 2008. **19**(3): p. 776-84.
128. Martina, J.A., et al., *MTORC1 functions as a transcriptional regulator of autophagy by preventing nuclear transport of TFEB*. Autophagy, 2012. **8**(6): p. 903-14.
129. Roczniak-Ferguson, A., et al., *The transcription factor TFEB links mTORC1 signaling to transcriptional control of lysosome homeostasis*. Sci Signal, 2012. **5**(228): p. ra42.

130. Raben, N., et al., *Suppression of autophagy permits successful enzyme replacement therapy in a lysosomal storage disorder--murine Pompe disease*. *Autophagy*, 2010. **6**(8): p. 1078-89.
131. Miedel, M.T., et al., *Membrane traffic and turnover in TRP-ML1-deficient cells: a revised model for mucopolidosis type IV pathogenesis*. *J Exp Med*, 2008. **205**(6): p. 1477-90.
132. Walkley, S.U. and M.T. Vanier, *Secondary lipid accumulation in lysosomal disease*. *Biochim Biophys Acta*, 2009. **1793**(4): p. 726-36.
133. Salaun, C., G.W. Gould, and L.H. Chamberlain, *Lipid raft association of SNARE proteins regulates exocytosis in PC12 cells*. *J Biol Chem*, 2005. **280**(20): p. 19449-53.
134. Kaushik, S., A.C. Massey, and A.M. Cuervo, *Lysosome membrane lipid microdomains: novel regulators of chaperone-mediated autophagy*. *EMBO J*, 2006. **25**(17): p. 3921-33.
135. Blott, E.J. and G.M. Griffiths, *Secretory lysosomes*. *Nat Rev Mol Cell Biol*, 2002. **3**(2): p. 122-31.
136. Rao, S.K., et al., *Identification of SNAREs involved in synaptotagmin VII-regulated lysosomal exocytosis*. *J Biol Chem*, 2004. **279**(19): p. 20471-9.
137. Yogalingam, G. and A.M. Pendergast, *Abl kinases regulate autophagy by promoting the trafficking and function of lysosomal components*. *J Biol Chem*, 2008. **283**(51): p. 35941-53.
138. Chen, F.W., C. Li, and Y.A. Ioannou, *Cyclodextrin induces calcium-dependent lysosomal exocytosis*. *PLoS One*, 2010. **5**(11): p. e15054.
139. Settembre, C., et al., *TFEB links autophagy to lysosomal biogenesis*. *Science*, 2011. **332**(6036): p. 1429-33.
140. Lieberman, A.P., et al., *Autophagy in lysosomal storage disorders*. *Autophagy*, 2012. **8**(5): p. 719-30.
141. Saftig, P. and J. Klumperman, *Lysosome biogenesis and lysosomal membrane proteins: trafficking meets function*. *Nat Rev Mol Cell Biol*, 2009. **10**(9): p. 623-35.
142. Rosenblatt, J.D., et al., *Culturing satellite cells from living single muscle fibre explants*. In *Vitro Cell Dev Biol Anim*, 1995. **31**(10): p. 773-9.

143. DiFranco, M., et al., *DNA transfection of mammalian skeletal muscles using in vivo electroporation*. J Vis Exp, 2009(32).
144. Louzao, M.C., et al., "*Fluorescent glycogen*" formation with sensibility for in vivo and in vitro detection. Glycoconj J, 2008. **25**(6): p. 503-10.